Review of Topologies, Application Areas, Modeling, and Control Methods for Switched Capacitor Circuits

Ting Yang, Lei Yang, *Senior Member, IEEE*, Bin Wu, *Student Member, IEEE*, Liangzong He, *Member, IEEE*, Yuanqi Zhang, Xinze Chen, Baoxiang Feng, Xiaojie Li, Haibing Wen, *Member, IEEE*, Jiaqiang Tian, *Member, IEEE*, Yaopeng Zhao, *Member, IEEE*, Mengying Hu, Jingjing Huang, *Member, IEEE*, Darui Zhu, Aimin Zhang, *Member, IEEE*, and Xiangqian Tong, *Member, IEEE*

***Abstract*—Switched capacitor (SC) circuits have been widely used for low-power and high-power areas, such as the integration circuit power supply, energy conversion for wearable devices, and power supply for data centers and electrical vehicles. The dc–dc conversion, dc–ac inversion, ac–dc rectification, and ac–ac conversion of SC topologies have been explored and discussed. This article provides a review of different topologies, application areas, mathematical models, and control methods for SC circuits. Compared with other review papers on SC converters, this article deeply and comprehensively surveys the topological structure classification and the equivalent circuits. It explores the application fields and the operation performance of SC circuits. The modeling method is presented as the steady-state modeling method and the transient modeling method. It will help to achieve accurate simulation and prediction and lay the foundation for theory analysis. The different mathematical models' construction algorithms and the suitable application range are analyzed in this article. The control methods determine the quality of the output voltage and the output power for SC circuits. They are classified as the linear control methods and the nonlinear control methods. The nonlinear control methods will help to achieve high-quality output voltage or current regulation with low ripples and fast dynamical response speed. The comparison of different topologies, application areas, modeling methods, and control methods is provided and discussed. What is more, the simulation accuracy of different modeling strategies and static and dynamical regulation performance of different control algorithms are presented in this article, respectively. The challenges and opportunities for SC circuits are prospected.**

***Index Terms*—Control method, modeling method, steady-state model, switched capacitor (SC) circuits, transient model.**

Manuscript received 30 August 2023; revised 11 November 2023; accepted 2 January 2024. Date of publication 5 January 2024; date of current version 16 February 2024. This work was supported in part by the National Natural Science Foundation of China under Grants 52107205, U2106218, and 52267019, in part by the 2023 Xi'an Science and Technology Plan Project under Grant 23GXFW0069, and in part by the Foundation of the International Science and Technology Cooperation Center of Renewable Energy and Hybrid Power, Shaanxi. Recommended for publication by Associate Editor Y. Siwakoti. *(Corresponding author: Lei Yang.)*

Ting Yang is with the School of Energy Engineering, Yulin University, Yulin 719000, China (e-mail: yt1028@yulinu.edu.cn).

Lei Yang, Yuanqi Zhang, Xinze Chen, Baoxiang Feng, Xiaojie Li, Haibing Wen, Jiaqiang Tian, Yaopeng Zhao, Mengying Hu, Darui Zhu, and Xiangqian Tong are with the School of Electrical Engineering, Xi'an University of Technology, Xi'an 710048, China (e-mail: yanglei0930@xaut.edu.cn; 1224165699@qq.com; 182579213@qq.com; 2224683100@qq.com; as1037247393@126.com; wenhb1989@hotmail.com; tianjiaqiang@xaut.edu.cn; ypzhao@xaut.edu.cn; hmy@xaut.edu.cn; zhudarui@xaut.edu.cn; xqtong@xaut.edu.cn).

Bin Wu is with the Analog Devices, Inc., Norwood, MA 02062 USA (e-mail: zjdaxwb@126.com).

Liangzong He is with the School of Aeronautics and Astronautics, Xiamen University, Xiamen 361102, China (e-mail: hlz190213@163.com).

Jingjing Huang and Aimin Zhang are with the School of Automation Science and Engineering, Xi'an Jiao Tong University, Xi'an 710048, China (e-mail: hjj7759@163.com; zhangam@mail.xjtu.edu.cn).

Color versions of one or more figures in this article are available at https://doi.org/10.1109/TPEL.2024.3350158.

Digital Object Identifier 10.1109/TPEL.2024.3350158

I. Introduction

SWITCHED capacitor (SC) circuits have demonstrated lightweight, small size, high power density, and minimized inductive switching loss or associated electromagnetic interference problems [1], [2], [3], [4], [5], [6], [7], [8], [9], [10], [11]. A pure SC converter consists of capacitors and transistor devices. The capacitors act as energy storage elements to achieve the power conversion or inversion capacity through a series and parallel connection [12].

A lot of SC topologies have been proposed and designed, allowing both dc–dc voltage step-up [13], [14], [15], [16], [17] and step-down [18], [19], [20], [21] functionality. What is more, the SC topologies are also designed for dc–ac rectification [22], ac–dc inversion [23], and ac–ac [24] conversion. The fundamentally different operation of SC circuits prohibits the use of classical analysis approaches adopted in magnetic-based converters. SC circuits are characterized by a voltage transfer ratio. The rational number is always determined by the topology. The transport power ability is related to an equivalent resistance determined by the operating frequency and the choice of components [25], [26]. The equivalent resistance of an SC circuit could be large, compared to effective impedances of inductor-based circuits. SC circuits amount to capacitors excited by voltage sources, while an inductor-based circuit incorporates capacitors excited by current sources.

The SC circuits have been widely used in the low-power area [27], [28], [29] and integration area [30], [31], [32]. The integrated SC capacitors could act as the power supply unit for the integrated circuit (IC) system on a chip and wearable devices [33], [34], [35], [36], [37], [38]. Some simple fully integrated SC circuits are already available in research labs and markets. However, as the equivalent circuit is mainly composed of resistors and capacitors, large charge current and discharge current spikes occur, which will damage the transistors and diodes, as shown in Fig. 1(a). For high-power-level applications, the small

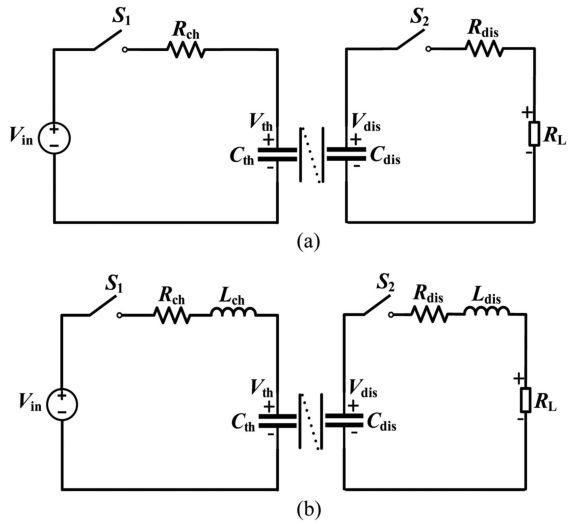

Fig. 1. Equivalent circuit for the SC converter and resonant SC converter [56]. (a) Equivalent circuit of the SC converter. (b) Equivalent circuit of the resonant SC converter with injected inductors.

value inductors will be correspondingly injected into the charge and discharge loops for SC converters, as shown in Fig. 1(b), to form a resonant inductor, in which the inductor resonates with the capacitor to achieve soft switching and suppress the current spikes for the switching devices. In this way, the SC converters could be used for the high-power application area [39], [40], [41], [42], [43], [44], [45], [46], [47]. It could provide high efficiency, high power density, and lightweight features.

To promote wide applications and easy voltage conversion control, it is essential to gain a full understanding of the SC circuits by using equivalent accurate models [38], [39], [40], [41], [42], [43], [44], [45], [46], [47], [48], [49], [50], [51], [52], [53], [54]. The state-space averaging (SSA) method is proposed for modeling SC circuits. It has become a standard method for switching capacitor circuit analysis [55]. The steady-state model of the SC circuit has been widely referred to as equivalent circuits for an equivalent resistance. Instead of deriving the conversion ratio of an SC circuit directly, the calculation of equivalent output impedance R_{eq} is explored. Some accurate steady-state modeling techniques based on transient calculation for simple dual-phase SC topologies are studied, especially for interleaved structures. However, no general modeling results are derived. The transient calculation-based modeling technique, which takes the output capacitor effect into account, is proposed, aiming to improve accuracy for output ripple analysis. It is based on the charge-balance transient-calculation (CT) modeling method [56]. The transient modeling method has been developed based on one switching cycle energy balance principle, as shown in [57] and [58]. It presents a dynamic capacitor ampere-second balance transient calculation (CASBTC) modeling method for SC circuits. This modeling method could accurately predict the steady-state and dynamic performance of an SC circuit. The instantaneous input voltage, output voltage, voltage of the flying capacitor, "ON time" of a transistor, "OFF time" of a transistor, or one switching cycle time are all included in the proposed model. The dynamical states of an SC circuit are continuously mirrored by the core model equation. Based on this modeling method, in combination with the variable frequency control method, the external disturbance could be instantaneously rejected by only adjusting the switching "OFF time" or one switching cycle time (switching frequency).

To explore the linear and nonlinear phenomena of power conversion, inversion, or rectification circuits, it is demanded to put forward some appropriate modeling methods. There are two main methods to study the complex behaviors in power conversion, inversion, or rectification circuits, including the exact simulation model and the iterative discrete map. The simulation model could derive all the operating behaviors in power conversion, inversion, or rectification circuits. However, an iterative discrete map could be adopted to analyze the stability of the system [59]. For inductor-based power conversion circuits, the steady-state modeling methods are widely used for circuit modulation, such as the circuit-averaging modeling method and the SSA modeling method [60], [61], [62], [63], [64], [65], [66]. In addition, many simplifications are considered due to the complexity added by the coupled inductor, the several operation stages, and the large number of energy storage elements. One of the most common simplifications is the assumption of a perfect magnetic coupling between the windings of the coupled inductor. An accurate dynamical small-signal model is constructed by modeling the equivalent resistors, as shown in [67]. Based on the analysis of the duty cycle loss caused by leakage inductance in the static gain of the inductor-based power conversion circuits, the equivalent resistors are derived. The linear and nonlinear performance study of SC circuits could refer to the inductor-based power conversion circuits by considering the charge and discharge features of the flying capacitor.

Different modeling methods have been proposed, including the steady-state modeling methods and the transient modeling methods for SC circuits. However, the different features are not compared. The suitable application area has not been figured out for the given model. This article will review the different kinds of mathematical models for SC circuits to set as the guidance for the simulation and the design of SC circuits. Many modeling methods considered the effects of capacitors and resistors in hard-switched SC circuits. The authors in [68] also considered the effects of stray inductance. It shows that the stray inductance could be a particular challenge in the design of complex or compound SC architectures. It proposes equations that could predict the rise of equivalent resistance due to stray inductance at high switching frequencies. A convenient curve fit based on the fast-switching limit (FSL) and the slow-switching limit (SSL) is presented as well.

The control method could determine the quality of SC circuits and has been highly developed [69], [70], [71], [72], [73], [74], [75]. For the low-power SC circuit, there are several kinds of control methods being used to achieve the output voltage regulation. Adopting the open-loop control method, the SC-based circuit could provide high power density with the simple circuit including switches and capacitors. However, the output voltage regulation of this kind of SC circuit is poor. It has a narrow input voltage and load operation range and suffers from

a structurally predetermined voltage conversion ratio. When it comes to high-power SC circuits, there are a few control methods presented in the literature. The unregulated control method is the common control method for high-power SC circuits. A proportional–integral (PI) control method is adopted for a 3X two-switch boosting SC (TBSC) converter. Based on the CT modeling method and peak current stress estimation, stable output voltage regulation is achieved for a high-power-level SC circuit. In some literature works, the inductive elements along the charge loops and discharge loops are adopted to change an SC circuit to a resonant SC circuit and to mitigate the current pulsation. The introduction of an inductive element is helpful in suppressing the peak charging current and to improve system efficiency with the soft switching operation [76], [77], [78], [79], [80], [81], [82], [83], [84], [85].

The rest of this article is organized as follows. Section II presents the topologies of SC circuits. The application areas of SC circuits are provided in Section III. Section IV shows the surveyed modeling methods for SC circuits. The control methods for SC circuits are shown and discussed in Section V. The conclusions and discussions are derived in Section VI.

II. Topologies of Switched Capacitor Circuit

There are different topologies of the SC circuit. Generally, the SC circuits could be divided into pure SC circuits, resonant SC (ReSC) circuits or hybrid SC (HSC) circuits, and quasi-SC (QSC) circuits. A majority of SC circuits operate with hard-switching and suffer the inrush charging current problem of capacitors. This seriously restricts performance improvement and application. To overcome this issue, the ReSC circuit introduces a small value inductor which is injected into the charge path or discharge path of capacitors. It develops a basic SC unit to an ReSC unit to achieve the soft switching [zero voltage switching (ZVS); zero current switching ZCS)]. The detailed comparison of different topologies of SC circuits is presented in Table I.

A. Pure SC Circuit Topology

SC circuits could provide the dc–ac inversion, dc–dc conversion, ac–ac conversion, and so on [24], [42], [86], [87], [88], [89], [90] with only capacitors and switches.

Marusarz [22] proposed a low-harmonic, 60 Hz sinusoidal 110 V ac from a 24 V dc source without inductors or transformers. The circuit topology allows the same power MOSFETs that sequentially charge a bank of capacitors to synthesize the staircase sine wave approximation. A Fourier analysis of the effects of MOSFET on-resistance and switching time on a 1-kW SC circuit prototype is conducted.

The authors in [91] and [92] proposed a TBSC converter. It distinguishes itself from the prior arts by symmetrically interleaved operation, reduced output ripple, low yet even voltage stress on components, and systematic expandability. A modeling method is formulated. The voltage regulation could be achieved through duty cycle and frequency adjustment. What is more, it also provides guidance for circuit components and parameter selection. A 1 kW TBSC converter is built to demonstrate the converter feasibility, regulation capability with duty cycle, and frequency control method. The peak efficiency of 97.50% is reached at the rated power. Sarafianos and Steyaert [93] presented a modified Dickson converter to achieve a wide input range capacitive dc–dc conversion. This converter has been implemented in a 90 nm technology, achieving a maximum output power of 50 mW and a peak efficiency of 76.60% in a 2:1 conversion mode. A multiratio helical ladder SC converter for low-power sensor nodes and a ladder SC converter are respectively presented in [94] and [95]. The authors in [96] proposed an (n/m)X SC converter. A 1-kW experimental prototype of a variable (4/0.5) is built with the boosting function. A peak measured efficiency of over 95% is achieved for the 1-kW experimental prototype.

The pure SC topology has acted as the ac–ac converter in [97] and [98]. A symmetrical SC multilevel ac–ac converter is presented in [42]. The SC technology is introduced into the ac–ac converter, which has the advantages of small size, high efficiency, and high power density. A 300-W prototype is built to verify the proportional relationship between input voltage and output voltage. The authors in [97] proposed a direct three-phase ac–ac converter based on the SC principle and ladder structure. With the bidirectional topology, the proposed converter could operate as a step-up or step-down ac–ac converter. The 95.10% efficiency of step-up and step-down modes, 0.94 capacitive power factor, and 96.00% output voltage regulation are achieved at the rated power. A bidirectional three-phase direct ac–ac converter, with only capacitors and switches in its power circuit and with its operation based on the SC principle, is proposed in [98]. The proposed ac–ac topology could convert ac–ac voltages within a wide frequency range, including dc voltage. A 6-kW prototype (1.35 kW/kg power density) has been designed and fabricated with the 380/110 V voltage conversion ratio and 100 kHz switching frequency. The measured efficiency at rated power is 96.30%. The topology of the presented bidirectional three-phase direct ac–ac converter is shown in Fig. 2.

B. Hybrid SC Circuit Topology

An HSC converter, along with its soft-charging and discharging feature, is illustrated to address the fundamental limits of conventional SC circuits and to efficiently utilize the high energy density of capacitors. What is more, in some literature works, the inductor-based converter topology and the pure SC converter topology will be combined together to achieve soft switching and high power density. On top of that, various SC topologies are synthesized from a single unit cell for obtaining higher conversion ratios. A 6:1 cascaded series–parallel (SP) merged with a multiphase interleaved buck topology is proposed in [99]. It presents a 48–1.5 V high step-down HSC converter. A 50-A prototype based on this topology is constructed. It achieves 90.24% efficiency. The authors in [100] proposed a nonisolated HSC dc–dc converter based on a modular multilevel converter. Its unidirectional structure is examined through circuit analysis. The voltage static gain is independent of the number of submodules. It provides a good regulation range of the output voltage for high-voltage (HV) applications. The experiments are conducted with a 1666-W prototype. A double input-parallel-output-series

TABLE I
TOPOLOGIES OF SC CONVERTERS

	Work	Function	Type	Inductors	Power Level and power density	Soft Switching	Efficiency (Maxi.)	Voltage Ripple or power factor	Input and Output Ports
Pure SC converter	[86]	Step-down	Normal	0	12.5 W, /	Nope	85.00%	0.50%	Single
	[87]	Step-down	Normal	0	10 W, 23 W/in^3	Nope	80.00%	/	Single
	[22]	DC-AC	SCPC	0	1000 W, /	Nope	/	/	Single
	[88]	Step-up	Serial-Parallel	0	/, /	Nope	93.00%	4.19%	Single
	[89]	Step-up	Fibonacci	0	27 W, /	Nope	88.00%	0.50%	Single
	[42]	Step-up/down	*N*-Level Bidirectional	0	1000 W, /	Nope	98.00%	4.00%	Bidirectional
	[90]	Step-down	N Stage	0	50 W, /	Nope	77.00%	/	Single
	[24]	AC–AC	Multi level	0	300 W, /	Nope	/	5.00%	Single
	[91]	Step-up	TBSC	0	1000 W, /	Nope	97.50%	/	Single
	[93]	Step-down	Dickson	0	50 mW, 16.3 mW/mm^2	Nope	76.60%	/	Single
	[94]	Step-down	HLSC	0	＜10 mW, 7.56 mW/mm^2	Nope	81.00%	/	Single
	[95]	Step-down	Ladder	0	24.6 W, 23 W/cm^3	Nope	93.50%	/	Single
	[96]	Step-up	Variable (n/m)X	0	1000 W, /	Nope	⩾95.00%	/	Single
	[97]	AC–AC, step-up and step-down	SC principle and ladder structure	0	3500 W, 0.787 kW/kg and 0.591 kW/L	Nope	⩾95.00%	PF⩾ 0.940	Bidirectional
	[98]	AC–AC	Three-phase bidirectional direct ac–ac topology	0	6000 W, 1.35 kW/kg	Nope	⩾96.30%	PF⩾ 0.969	Bidirectional
HSC Converter	[99]	Step-down	6:1 Cascaded Series–Parallel	3	75 W, /	Nope	90.24%	/	Single
	[100]	Step-down	MMC	1	1666 W, /	Nope	/	1.00%	Single
	[101]	Step-up	Double Input-Parallel-Output-Series	2	120 W, /	Nope	95.00%	/	Double Input
	[102]	Step-down	Hybrid ReSC	6	440 W, 26.44 mW/mm^2	ZCS	96.30%	/	Single
	[23]	AC-DC	Three-phase multilevel HSC	1	7500 W, /	/	97.78%	/	Single
	[103]	AC–AC, step-up	Hybrid inductive switching cell and SC ladder cell	1	1 kVA, 1.48 kW/kg and 0.95 kW/L	/	93.00%	PF=0.97 4	Single
Resonant SC Converter	[104]	Step-down	Cascade	2	720 W, 2500 W/in^3	ZVS	99.00%	3.0%	Single
	[105]	Step-up	N Dickson	1	150 W, /	ZVS	90.00%	/	Single
	[106]	Step-up	Three Level	1	500 W, /	ZVS	95.00%	/	Single
	[107]	Step-down	Series-Parallel	3	600 W, /	/	95.50%	/	Single
	[108]	Step-down	Half-Bridge Cell	1	3500W, /	ZCS	≥98.00%	/	Single
	[109]	Step-up	RTBSC	1	140 W, /	ZVS and ZCS	98.30%	/	Single
	[111]	Step-up	SP-MRSCC	4	100 W, /	ZCS	94.40%	/	Single
	[112]	Step-up/down	PSCs and OSCs	2	＜150 W, /	/	/	/	MIMO
	[113]	DC-AC	SC-MLIs	1(5 level), 2(7 level)	/	ZVS	⩾98.40%	1.41%	Single
	[114]	AC-DC	Three-phase RSC	4	216 W, 3.93 W/cm^3	ZCS	⩾98.00%	Current ripple: 10.00%	Single
QSC Converter	[115]	Step-up	N-Stage	0	30 W, 15 W/in^3	/	78.00%	/	Single
	[116]	Step-up	QSC cells	0	20 W, 10 W/in^3	/	74.00%	/	Single
	[117]	Step-up/down	Bidirectional QSC	2	1000 W, /	ZCS	Buck:＞ 92.00% Boost: ＞ 82.00%	/	Bidirectional
	[118]	Step-down	Dual Basic QSC	0	36 W, 20W/in^3	/	73.00%	/	Single

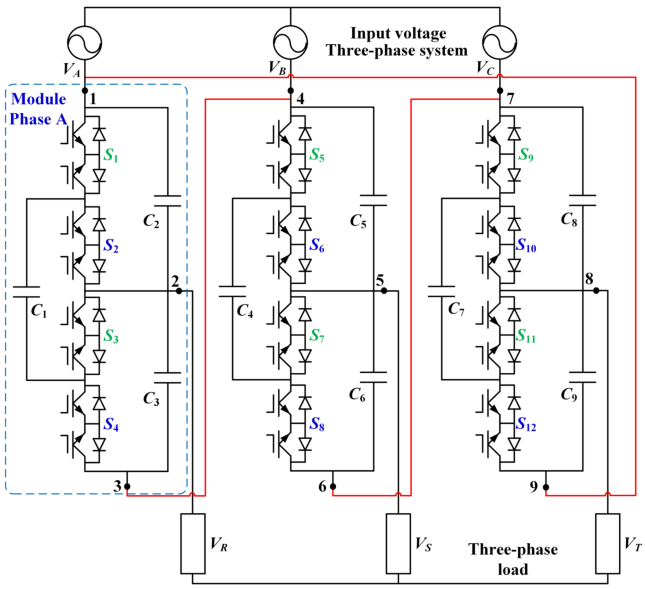

Fig. 2. Three-phase bidirectional SC AC–AC converter in [98].

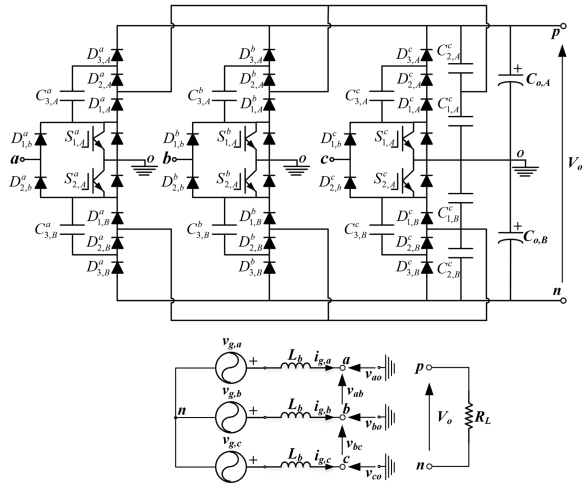

Fig. 3. High-gain three-phase multilevel HSC PWM PFC rectifier in [23].

hybrid SC boost (DIPOS-HSCB) converter is proposed, which consists of two different kinds of input-parallel-output-series circuits as shown in [101]. The proposed DIPOS-HSCB converter achieves an HV gain with low component stress and a small input current ripple. Furthermore, an automatic current balancing function for all input inductor currents could be achieved using a special carrier phase-shifted modulation scheme. The prototype rated at 200 V/120 W is built and the maximum efficiency of the proposed DIPOS-HSCB converter is 95.00% at 120 W. The authors in [102] proposed a novel hybrid ReSC converter that performs a 48–3.4 V direct conversion. The prototype of the proposed converter is constructed for theory verification. It provides a continuous output power of 440 W with a maximum efficiency of 96.30% at 30 A load current.

The HSC topology is adopted for ac–dc power rectification or ac–ac power conversion. Cortez and Barbi [23] proposed a three-phase multilevel power factor correction rectifier using the HSC concept. It achieves good features such as low number of active switches, HV gain (ac–dc), sinusoidal currents, low voltage stress across all components, and simple control. A 7500 W/220 V to 1600-V laboratory prototype is built and tested. It provides 97.78% maximum power rectification efficiency. The proposed topology is shown in Fig. 3. A hybrid boost SC converter operating as an ac–ac solid-state autotransformer is presented in [103]. The high-gain ratio output voltage could be obtained by integrating a basic inductive switching cell and an SC ladder cell. A single-phase prototype is constructed with 55/220 V voltage conversion and 1 kVA rated power. The measured 93.00% peak efficiency is achieved with the 0.974 power factor.

C. Resonant SC Circuit Topology

In combination with other potential advantages such as soft switching and voltage regulation, resonant SC converters are developed. In the ReSC approach, both inductors and capacitors are used in the voltage conversion and power transfer process. It shows promise in the development of future high-performance power electronics systems. Compared to conventional SC converters, the augmenting inductors can greatly reduce or eliminate the capacitor charge sharing loss, and thus improve the energy utilization of the capacitors without sacrificing efficiency. The cascade topology, N Dickson topology, and three-level topology ReSC converter are, respectively, presented in [104], [105], and [106]. The ZVS function is achieved. An improved 48–12 V step-down SP ReSC converter for data center applications is presented in [107]. The 95.50% peak efficiency is achieved with a proper switching device voltage clamping strategy. A special ReSC converter is shown in [108] with the ZCS function. It possesses features such as high efficiency, high power density, and lightweight. ZCS could be achieved with the resonant operation. It allows the converter to operate with high efficiency. A family of resonant two-switch boosting switched-capacitor converters (RTBSCs) with ZVS operation and a wide line regulation range is proposed in [82], [109], and [110]. Based on the previously proposed TBSC converters in [90] and [91], only a small resonant inductor is added, while two bulky capacitor banks are replaced by two small-value resonant capacitors. Furthermore, by operating an RTBSC converter above the resonant frequency, the transistors are ZVS turned ON and diodes are ZCS turned ON/OFF. The authors in [111] proposed a kind of SP multiresonant SC converters (MRSCCs) by incorporating resonant tanks into the traditional SP-SC converter and adopting the on-time fixed frequency modulation. A 100-W 4X SP-MRSCC prototype is designed and tested to verify the above analyses. It has the potential to be utilized for connecting 12 V and 48 V dc buses between traditional and future data centers. A generalized synthesis methodology is proposed in [112] to derive multi-input multioutput (MIMO) converters without intermediate energy buffer stages based on basic power converter cells. The authors in [113] introduced the ZVS technique into SC-based multilevel inverters (MLI) by updating the basic SC unit to the resonant

TABLE II
APPLICATION AREAS OF SC CIRCUITS

Work	Function	Type	Power Level	Efficiency (Maxi.)	Load Voltage	Operated Frequency	Application Area
[119]	Step-down	Resonant SC Converter	600 W	98.55%	9.0 V	387 kHz	Data Center
[120]	Step-down	ZIV Converter	840 W	99.00%	12.0 V	60 kHz	
[121]	Step-down	HSC Converter	750W	97.50%	5.1 V	450 kHz	
[122]	Step-down	Resonant SC Converter	720W	99.00%	12.0 V	100 kHz	
[123]	Step-up	Four-level flying-capacitor converter	55 kW	⩾97.00%	660.0 V with 220 V input voltage(Maxi.)	8 kHz , 12 kHz, and 20 kHz	Electric Vehicle
[124]	Step-up	Resonant SC Converter	/	97.00%	400.0 V	20 kHz	
[125]	Bidirectional	HSC Converter	400 W	Step-up: 94.09%; Step-down: 94.41%	Forward:400.0V Reverse:40.0-120.0 V	20 kHz	
[126]	Step-up	SQBC	300 W	97.83%	300.0 V	36 kHz	
[127]	Step-down	ID	<0.2 W	87.00%	1.1 V	/	IC power supply
[128]	Step-down	GSwRC	2.25 W	85.00%	1.5 V	5 MHz	
[129]	Step-down	2:1 ReSC	7.7 W	85.10%	3 V, 1.85 V	50–60 MHz	
[130]	Step-down	3:1 ReSC	4.62 W	87.00%	3.7 V	1.7 MHz	
[131]	Step-up	Charge-Pump Voltage Doubler	0.125 W	81.70%	5 V	31.25 kHz to 1 MHz	
[132]	Step-down	Multiphase SC Converter	1 W	80.00%	1.2 V–3.3 V	/	
[133]	Step-up	HSC Converter	500 W	97.00%	58.0 V	100 kHz	PV Strings
[134]	/	SCC-Based Modular DPP	60 W (each panel)	99.60%	≈31.0 V	100 kHz	
[135]	1:3, 1:4, 1:5, 1:6, and 1:7	SPV	0.17~1.7 mW (PV cell)	93.70%	0.5–2.2 V (PV cell)	1 MHz	
[136]	Step-up/down	Pure SC Converter	1.5 mW	98.00%	3.7 V, 1.2 V, 4.9 V, and 2.5 V	1.1 MHz	Wearable Devices
[137]	Step-down	DOSC	300 μW	78.00%	1.0 V and 0.55 V	13 MHz	
[138]	Step-up/down	Parallel SC with Time Multiplexing	190 μW	95.80%	0.1–1.9 V	10 kHz	
[139]	Step-down	Multiple Voltage Gain SC Buck Converter	40 μW	80.00%	1 V, 0.8 V, and 0.6 V	13 MHz	
[140]	Step-down	Fully Integrated Asynchronous	1–230 μW	80.00%	0.3–1.1 V	/	

SC unit. Experimental results of both five-level and seven-level SC inverters demonstrate the effectiveness of the ZVS design.

The authors in [114] proposed a three-phase resonant driver based on the ReSC for the light-emitting diode (LED). The proposed ac–dc resonant SC LED driver provides good features, such as low current ripple and low flicker. The ZCS is achieved. A 216-W laboratory prototype is designed to supply an LED device from an ac 220 V (60 Hz) voltage source. The experimental results show that the power factor is higher than 0.98, with 6.60% flicker and 89.00% power rectification efficiency.

D. QSC Circuit Topology

The QSC converter, as shown in [115], [116], [117], and [118], has been proposed to achieve the continuous input current waveform and better regulation capability than the traditional SC circuits. The transistors of the QSC circuit are operated in an active region, acting as a voltage-controlled current source. The current magnitude is determined by the gate–source voltage.

III. APPLICATION AREAS OF SWITCHED CAPACITOR CIRCUITS

The SC circuits have been used for different areas such as data centers, electric vehicles (EVs), solar energy generation and harvesting, IC power supply, and wearable devices. The detailed application areas of SC circuits are given in Table II.

A. Data Center Application

A data center is typically a centralized location where all the networking and computing equipment is placed and connected for the purpose of gathering, processing, and mainly storing and allowing access to large amounts of data to the consumers. To

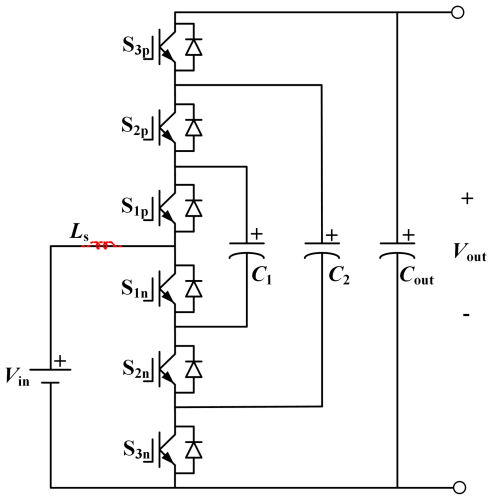

Fig. 4. Four-level flying-capacitor DC–DC converter [123].

the high-power consumption of data centers, the dc distribution system is widely used to replace traditional ac systems in data centers due to its high efficiency feature. To provide a solution to an ever-growing stress on data centers and their huge power losses, different topologies of SC circuits have been developed, such as the ReSC circuits [119], zero inductor–voltage (ZIV) circuits [120], and the HSC circuits [121]. A resonant SC converter is adopted for data center power conversion, as shown in [122]. It provides 99.00% peak efficiency. The ZVS control technique is implemented on the presented cascaded resonant-based intermediate bus converter (IBC) for 48–12 V data center power delivery with a 720-W hardware prototype.

B. Electric Vehicles Application

The SC circuit has been adopted for EVs for many years, as shown in [123], [124], [125], and [126]. A 55 kW variable 3X SC dc–dc converter for plug-in hybrid EVs is shown in [123]. The utilization of parasitic inductance in the proposed variable 3X converter reduces the pulse current, the conduction loss, and the capacitance requirement. A compact size (27.2 cm $\times$ 24.4 cm $\times$8.8 cm) and lightweight (5.6 kg) are achieved with more than 97.00% efficiency. The topology of the variable 3X SC converter is shown in Fig. 4. An HSC/switched-quasi-Z-source bidirectional dc–dc converter (SQBC) is proposed in [125] for EVs with hybrid energy sources. It has a wide voltage gain range in the bidirectional energy flows. Compared with the traditional quasi-Z-source bidirectional dc–dc converter, the proposed converter only changes the position of the main power switch and employs an SC cell at the output of the HV side. The forward 400 V dc voltage is achieved with 94.09% peak efficiency. The reverse 40–120 V voltage could be reached with 94.01% peak efficiency. The SQBC has the characteristics of wide voltage gain and low voltage stress. It is suitable for the power interface between the supercapacitors and the dc bus in the multisource system of EVs. Based on the topology of SQBC, the authors in [126] achieved the ZVS ON for all power switches and ZCS OFF for synchronous rectification switches in both step-up and step-down modes by adjusting the switching frequency to adapt the boundary soft-switching condition. The peak 97.83% efficiency over a wide operation range is reached with a good dynamic response.

C. IC Power Supply Application

The integrated SC converter has been used for the IC power supply with high power density capacity and high integration capacity, as shown in [127], [128], [129], [130], [131], and [132]. A novel interleaved discharging (ID) approach is presented in [127] to reduce the output ripple in step-down SC dc–dc converters. The verification results of a four-stage SC dc–dc converter show that the ID approach could reduce the output ripple by a factor of three. The proposed ID topology also improves the converter efficiency by 7.00%. The authors in [128] presented a detailed analysis of the characteristics of a gyrator switched-resonator converter (GSwRC) IC. The optimization method combined with the converter's benefits presents an attractive approach for power delivery in point-of-load (PoL) applications. The fabricated IC prototype operation is demonstrated with 1.5 A, delivering up to 2.25 W from a 3 V input voltage, with peak efficiency at 85.00%. An IC implementation of an HSC converter based on a modified SP architecture is presented in [130]. The converter operates in a quasiresonant mode to regulate a nominal 3.7 V output voltage from a 12 V supply voltage. The presented converter IC is designed in 180 nm bulk complementary metal–oxide–semiconductor (CMOS) with a 5 V option for power devices. It is tested in a flip-chip assembly with a 36 nH 0402 inductor to deliver up to 4.6 W at 87.50% efficiency at a power density of 0.23 W/mm^3. The authors in [131] presented a 3–5 V integrated dual-mode digital-control step-up SC dc–dc power converter. The feedback control circuit is equipped with a low-power analog-to-digital converter that monitors and feeds the output voltage to a digital controller. With light loading, the control loop operates in a pulse-skipping mode. With heavy loading, the control loop operates in a frequency modulation mode based on a numerically controlled oscillator whose switching frequency varies from 31.25 kHz to 1 MHz. The presented design generates a regulated 5 V output voltage with an output current of up to 25 mA from a 3 V power supply, delivering an output power greater than 100 mW. The load regulation is measured to be 0.14% with an efficiency of 80.00%. The IC of the inductorless switched-mode dc–dc voltage converter is proposed in [132]. The converter is based on a novel multiphase SC architecture. It uses reconfigurable charge-pump circuits and a multiloop discrete and continuous time control technique. It is used as a stand-alone IC for converting power rail voltages or lithium electrochemical cell voltages 2.8–5.5 V into power supply voltages 1.2–3.3 V of the modern microcontrollers and other low-voltage ICs.

D. Solar Power Generation and Solar Energy Harvesting Application

SC circuit is also adopted for solar power generation and solar energy harvesting. The authors in [133] proposed the SC-based

integrated pulsewidth modulation (PWM) boost converter integrating voltage equalizer for the photovoltaic (PV) strings. The presented integrated converter could control the operation voltage of a string while automatically preventing the partial shading issues, hence achieving two functional roles at the same time. The peak 98.00% efficiency is achieved with the 500 W power level. The authors in [134] introduced a switched-photovoltaic (SPV) dc–dc converter that switches the PV cells of a series solar string periodically in parallel to balance their voltages and extract the maximum available power under mismatch conditions. This SPV converter exploits the intrinsic capacitance of the PV cells to establish an implicit 1:n SC converter that allows the extra current of the stronger cells in the string to flow around the underperforming cells to the output instead of getting shunted to the ground. Fabricated in a 0.18 μm CMOS process, the presented SPV converter achieves a peak harvesting efficiency of 91.30% under 50% current mismatch among the employed PV cells, demonstrating a 30.20% efficiency improvement over the prior solutions. An SC-based integrated PWM boost converter integrating voltage equalizer is proposed in [135]. The proposed integrated converter could control the operation voltage of a string while automatically preventing the partial shading issues, hence achieving two functional roles at the same time. The experimental equalization tests for three panels connected in series are performed emulating a partial shading condition with a 500 W prototype. The verification results show that the string voltages could be boosted based on the PWM control method. The prototype achieves a 21.00% improvement in extractable maximum power. Thus, it demonstrates the efficacy of the proposed integrated converter.

E. Wearable Devices Application

SC circuits have been widely used for wearable devices. The authors in [136] proposed an SC converter that could achieve the step-up and step-down voltage conversions of 3.74 and 1.233 V for normal mode and 4.87 and 2.48 V for high mode, with the ripple variation of 20–60 mV. The proposed converter has been designed in a standard 0.35 μm CMOS technology and with conversion efficiency up to 97.00%–98.00%. It agrees with state-of-the-art SC converter designs. The authors in [137] presented an area and power-efficient dual-output switched capacitor (DOSC) dc–dc buck converter for wearable biomedical devices. This DOSC converter has an input voltage range between 1.05 and 1.40 V and generates two simultaneous regulated output voltages of 1 and 0.55 V. A step-up/step-down unified topology is proposed in [138] which covers the input voltage range from 0.85 to 3.6 V and the output voltage range from 0.1 to 1.9 V. A dual-output topology with a four-way channel mapping and an on-demand channel sharing control is also presented and verified for delivering two regulated voltages with good efficiency and fast transient response speed. The authors in [139] introduced an efficient reconfigurable, multiple voltage gain SC dc–dc buck converter as part of a power management unit for wearable electronics. The proposed SC converter achieves an input voltage of 0.6–1.2 V generated from an energy harvesting source. The presented SC converter utilizes pulse–frequency modulation to generate multiple regulated output voltage levels, namely 1, 0.8, and 0.6 V based on two reconfigurable bits over a wide range of load currents from 10 to 800 μA. The measured peak efficiency is 80% at a load current of 800 μA and regulated load voltage of 1 V. A fully integrated asynchronous step-down SC dc–dc conversion structure suitable for supporting ultra-low-power circuits commonly found in biomedical implants is presented in [140]. The designed circuit regulates load voltages from 300 mV to 1.1 V derived from a 1.2 V input voltage. A total of 350 pF on-chip capacitance is implemented to support a maximum of 230 μW load power while providing efficiency up to 80%. The validated circuit of the proposed concept is fabricated in 0.13 μm CMOS technology. Experimentally measured results confirm the expected functionality and performance of the proposed circuit.

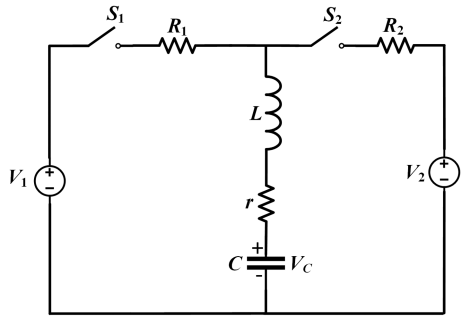

Fig. 5. SC topology for model analysis.

IV. Modeling Methods for Switched Capacitor Circuits

In the modeling methods of switching capacitor circuits in general, and power stages in particular, two main approaches are presented: one is based on state-space modeling, and the other uses an averaging technique, as shown in [55]. There are several steady-state modeling methods for SC circuits. The previous modeling methods for SC circuits have established static models essentially composed of an ideal transformer and an equivalent output resistance (EOR). Recently, some transient modeling methods have been proposed to simulate the dynamic performance of an SC circuit.

A. Average Current-Based Method

In [141] and [142], an average current-based steady-state model is proposed based on Fig. 5. It assumes the intermediate capacitor voltage varying from V_{c1} to V_{c2} during the discharging state. According to the charge balance principle, the average current passing from V_1 to V_2 is found and defined as i.

The equivalent resistance between V_1 and V_2 is thus derived as follows:

$$R_{\text{eq}} = \frac{V_1 - V_2}{i} = \frac{1}{fC}\frac{1+\exp(\frac{DT}{\tau})}{1-\exp(\frac{DT}{\tau})} \tag{1}$$

where D is duty cycle of charging and discharging states, and $\tau = RC$ is the time constant of charging and discharging loops.

Equation (1) provides a unified form of the output impedance showing the overall impacts of circuit parameters on the steady state of the unity gain SC converter, including the switching frequency, duty cycle, time constant, and capacitance of the flying capacitor. However, the method is based on the assumption of firm input and output sources. It is general but may not be accurate when a limited output filter capacitor is considered.

All impacts of the circuit of steady-state SC circuits are exhibited by (1), including capacitance of the flying capacitor, switching frequency, duty-cycle, and charging and discharging constants. However, due to the loss estimation of the average current, the accuracy under low frequency is impaired, as shown in [142].

The average current-based method has been used for the resonant SC converter, as shown in [142]. The circuit is simplified to a lumped *RLC* circuit, as shown in Fig. 3. This circuit is used to describe the operation of each subcircuit in its relevant conduction time. To comply with the equivalent model, the equivalent resistance of the substate of resonant SC converters could be derived as

$$R_{eia} = k_{\mathrm{i}}^2 \frac{\pi R_{ia}\varphi_i}{4df_i}[1 - \sin c(2\varphi_i)] \tag{2}$$

where k_{i} is the proportionality factor of the charge phase, the angle $\varphi_i = \pi T_{ia}/T_i$, T_{ia} is the time interval, $df_i = f_s/f_{0i}$ is the ratio between the switching frequency and the natural frequency of the resonant network, and R_{ia} is the substate loop resistance.

The power loss of the substate could be expressed as a function of the average output current as

$$P_{eia} = (I_o)^2 k_i^2 \frac{\pi R_{ia}}{4df_i}[\varphi_i - \cos(\varphi_i)\sin(\varphi_i)]. \tag{3}$$

The energy dissipated in the subcircuit due to the loop resistance R_{ia} and the current during the time interval T_{ia}, which is derived by integrating the instantaneous power over the substate time interval T_{ia}, is derived as

$$\begin{aligned} E_{ia} &= R_{ia}(I_{pki})^2 \int_0^{\varphi_i/\omega_{0ia}} k_i^2[\sin(\omega_{0ia}t)]^2 dt \\ &= R_{ia}(I_{pki})^2 \frac{[\varphi_i - \cos(\varphi_i)\sin(\varphi_i)]}{2\omega_{0ia}} \end{aligned} \tag{4}$$

where $\omega_{0ia} = 2\pi f_{0ia}$ is the natural resonant frequency of the phase *i* substate "a."

B. Average-Current-Base Conduction Loss Method

Another general method based on average-current conduction loss calculation is presented in [143]. This method divides a switching period into switching phases according to the operation modes. For each phase, equivalent *RC* subcircuits are found and the power loss caused by each subcircuit is calculated to match a corresponding equivalent output resistor R_{eq}. Then, the total output impedance can be accumulated as follows:

$$R_{\mathrm{eq}} = \sum_{i=1}^{M} k_i^2 \frac{1}{2f_s C_i} \frac{1+\exp(\beta_i)}{1-\exp(-\beta_i)} \tag{5}$$

where $\beta_{\mathrm{i}} = T_{\mathrm{i}}/R_{\mathrm{i}}C_{\mathrm{i}}$, $T_{\mathrm{i}} = 1/f_{\mathrm{i}}$ is the operation time of the subcircuit, R_{i} is the total resistance alone the circuit loop, C_{i} is the total capacitance, and k_{i} is the proportionality factor that is calculated by *KCL* principle taking into account the charge balance equations.

This method could be used for either dual-phase SC circuits or multiphase SC circuits. It also considers the frequency effect on the steady state. However, it suffers from inaccuracy issues for SC circuits with large capacitor voltage ripple for its employment of average current for conduction loss calculation. This method is suitable for SC circuits without coupling loops since the *RC* subcircuits are difficult to simulate for some complex SC circuits. Complex coupling loops refer to two circuit loops which share a common element while each loop contains individual charging and discharging elements (source or capacitor) in the same switching mode. A typical example is the ladder SC converter.

C. State-Space Averaging Method

An SSA model is proposed in [144] and [52], and the EOR is derived as

$$R_{\mathrm{eq}} = R + \frac{R}{2d} \tag{6}$$

where $R = R_{\mathrm{on}} + r$, R_{on} is the "ON resistance" of the transistor, r is the internal resistance of the flying capacitor, and d is the duty-cycle of the charging period of the flying capacitor.

As shown in (6), the SSA modeling method is focused on the duty cycle of switches, and the accuracy will be affected by the capacitance of the flying capacitor and the "ON time" of the charging period.

The state-space modeling technique has also been applied here to estimate the variation in EOR for different operating conditions of multilevel SC circuits using the pulse-dropping switching scheme.

The maximum and minimum values of the SSL for an *N*-module multilevel SC converter are shown in the following equation:

$$R_{\mathrm{SSL,min}} = \frac{N}{Cf_{\mathrm{sqr}}} \tag{7}$$

$$R_{\mathrm{SSL,max}} = \frac{N}{Cf_{\mathrm{tri}}} = \frac{N \times m_{\mathrm{f}}}{C \times f_{\mathrm{sqr}}} = m_{\mathrm{f}} \times R_{\mathrm{SSL,min}} \tag{8}$$

where f_{sqr} and f_{tri} are the frequency of the square and triangular waves, respectively; m_{f} is the frequency modulation index.

The EOR of the *N*-module multilevel SC converter is derived as

$$R_{\mathrm{eq}} = \frac{(N+1)V_{\mathrm{in}} - V_{\mathrm{out}}}{i_{\mathrm{out}}}. \tag{9}$$

The averaged-switch modeling method considers conduction losses in a discontinuous mode for SC circuits, as shown in [144] and [52]. It proposes a dynamic average-value model of the capacitor-based switching stage in fourth-order PWM dc–dc converters. The power dissipation due to conduction loss is also considered. The average-value models of dependent sources could be derived by considering the functions of the duty cycle

and average values of switching-stage terminal variables. The conduction loss of the averaged capacitor-based stage should dissipate the same power as the respective parasitic. The total resistance and voltage source representing the combined parasitic is calculated as

$$r_{\text{tot}} = r'_{\text{sw}} + \frac{\left[(\bar{i}_{L1}+\bar{i}_{L2})(1-d_1)+\bar{i}_{L1}d_2\right]^2}{\left[(\bar{i}_{L1}+\bar{i}_{L2})(d_1-d_2)+\bar{i}_{L1}d_2\right]^2} r'_{fd} + \frac{\left[\bar{i}_{L2}(d_1-d_2)+\bar{i}_{L1}(1-d_1)\right]^2}{\left[(\bar{i}_{L1}+\bar{i}_{L2})(d_1-d_2)+\bar{i}_{L1}d_2\right]^2} r'_{C_1} \tag{10}$$

$$V_{\text{tot}} = \frac{(\bar{i}_{L1}+\bar{i}_{L2})(1-d_1)+\bar{i}_{L1}d_2}{(\bar{i}_{L1}+\bar{i}_{L2})(d_1-d_2)+\bar{i}_{L1}d_2} V_{fd}. \tag{11}$$

D. FSL and SSL Methods

The SSL and FSL modeling methods are proposed in [145]. For the SSL model, the finite resistance of a transistor and the equivalent series resistance of a flying capacitor are ignored, and the output resistance is derived as

$$R_{\text{SSL}} = \sum_i \frac{{a_{c,i}}^2}{c_i f_s}. \tag{12}$$

For the fast-switching frequency limit model, the output resistance is given as

$$R_{\text{FSL}} = 2\sum_i R_i({a_{r,i}}^2). \tag{13}$$

The slow and fast switching frequency limit modeling methods just emphasize the output impedance under very slow and fast switching frequency conditions. Based on the energy conservation principle, it neglects the parameter of the duty-cycle.

An accurate and generalized curvature-based, steady-state modeling technique for SC circuits is proposed in [146]. The proposed technique provides averaged expressions for all capacitor voltages across the full range of practical operating conditions, including the hybrid SSL-FSL mode. A simple and generalized expression for the output impedance is obtained, which relates the SSL and FSL impedances to the total output impedance. This expression could be used to quickly and accurately compute the output voltage without deriving the converter's state equations and to precisely weigh the contribution of each floating capacitor and parasitic resistance on the output impedance. The output impedance formula for the SC circuit could be written as

$$R_{\text{o}} = \frac{R}{D_1} + \frac{R}{D_2} + \frac{1}{Cf_s}\left[\frac{1}{1-e^{-D_1T_{\text{s}}/RC}} + \frac{1}{1-e^{-D_2T_{\text{s}}(C+C_{\text{out}})/RCC_{\text{out}}}} - \frac{RC}{D_1T_{\text{s}}} - \frac{RCC_{\text{out}}}{D_2T_{\text{s}}(C+C_{\text{out}})} - 1\right]. \tag{14}$$

E. Phase-Shift Modeling Method

A phase-shift modulation method is proposed for the GaN-based SC converter, as shown in [147]. The presented SC circuit could realize HV gain with high efficiency and power density based on its modular topology. The general steady-state model is built. The relationship between the order of the dynamic model based on the conventional method and the number of modules in the converter is achieved to illustrate the complexity and high computational cost.

F. Voltage Gap Calculation Method

Another modeling approach based on voltage gap calculation is shown in [148]. It is also based on the basic SC block, as shown in Fig. 2. The voltage gap between the input voltage and maximum flying capacitor voltage as well as the gap between minimum flying capacitor voltage and the output voltage is calculated. Based on the proposed gap expressions, the equivalent impedance between V_1 and V_2 could be expressed as follows:

$$R_{\text{eq}} = \frac{1}{Cf_{\text{s}}}\left(1 + \frac{e^{-\frac{T_{\text{Cr}}}{R_{\text{Cr}}C}}}{1-e^{-\frac{T_{\text{Cr}}}{R_{\text{Cr}}C}}} + \frac{e^{-\frac{T_{\text{dr}}}{R_{\text{dr}}C}}}{1-e^{-\frac{T_{\text{dr}}}{R_{\text{dr}}C}}}\right). \tag{15}$$

This modeling method is developed for multi-input SC circuits, regardless of resonant or nonresonant conditions.

G. Charge-Balance Transient-Calculation Method

The static states have been deeply studied in [149] and [150], and the transient calculation for SC circuits is also proposed. A CT modeling method is presented to address the regulatory challenges for SC circuits [53]. The accuracy of the model is improved by employing transient calculation. It takes the charge redistribution phase into account. What is more, the duty cycle, switching frequency, as well as output capacitor are also considered simultaneously in the final output impedance formula.

For the interleaved SC circuit condition, the EOR is derived as

$$R_{\text{eq}} = \frac{T_{\text{s}}}{4C_1}\coth\left(\frac{dT_{\text{s}}}{2R_{\text{ch}}C_1}\right) + \frac{C_oT_s}{4C_1(C_1+C_o)} + \frac{C_1}{C_1+C_o}R_{\text{dis}} \tag{16}$$

where C_1 is the capacitance of the flying capacitor and C_o is the capacitance of the filter capacitor, d is the duty cycle of charge switch, T_{s} is a period of one switching cycle, R_{ch} is the equivalent resistance of the charge loop, and R_{dis} is the equivalent resistance of the discharge loop.

For the noninterleaved SC circuit condition, the EOR is given as

$$R_{\text{eq}} = \frac{T_{\text{s}}}{2C_1}\coth\left(\frac{dT_{\text{s}}}{2R_{\text{ch}}C_1}\right) + \frac{(2C_o+C_1)^2T_s}{8C_1C_o(C_1+C_o)} + \frac{C_1}{C_1+C_o}R_{\text{ch}}. \tag{17}$$

H. Dynamic Capacitor Ampere-Second Balance Transient Calculation Modeling Method

A dynamic CASBTC modeling method is proposed in [57] and [58], which is based on the work presented in [151] and

TABLE III
COMPARISON OF SURVEYED MODELING METHODS FOR SC CIRCUITS

Modeling Method	Pros	Cons	Voltage Gain (V_o/V_{in})	Output Impedance (R_{eq})	Suitable Application
Average Current-Based Method (AC)[141],[142]	Straightforward, for Simple Dual-Phase SCC	Not generalized, Infinite Output Capacitor Assumed	$\frac{T}{C}\frac{e^{\frac{d+0.5}{RC_1}T_s}-1}{(e^{\frac{dT_s}{RC_1}}-1)(e^{\frac{0.5T_s}{RC_1}}-1)}$	$\frac{V_1-V_2}{i}=\frac{1}{fC}\frac{1+\exp(\frac{DT}{\tau})}{1-\exp(\frac{DT}{\tau})}$	Simple Dual-Phase SC Converter
Average-current based Conduction Loss Method ACCL [143]	Generalized, Continuous Frequency Range Addressed	Inaccurate Under Large Capacitor Voltage Ripple	$\frac{T_s}{2C_1}\coth(\frac{dT_s}{2RC_1})+\frac{T_s}{2C_1}\coth(\frac{0.5T_s}{2RC_1})$	$\sum_{i=1}^{M}k_i^2\frac{1}{2f_sC_i}\frac{1+\exp(\beta_i)}{1-\exp(-\beta_i)}$	Dual-Phase and Multiphase SC Converter with Simple RC Loops
FSL and SSL methods (FSL-SSL) [145]	Generalized, Easy Implementation for Complex SCC	Inaccurate in Moderate Switching Frequency Region	/	$\begin{cases}R_{SSL}=\sum_i\frac{a_{c,i}^2}{c_if_s}\\R_{FSL}=2\sum_iR_i(a_{r,i}^2)\end{cases}$	Complex Dual-Phase SC Converter with Very High or Low Frequency
Phase-shift Modeling method [147]	GaN-Based SC Converter	Not Generalized, Infinite Output Capacitor Assumed	$V_L+(N-1)\sum_{k=1}^{M}V_k^*$	/	Dual-Phase SC Converters and Resonant SC Converters
Voltage-Gap Modeling Method (VG) [148]	Easy Implementation for Multi-Input SCC	Not Generalized, Infinite Output Capacitor Assumed	$\frac{T}{C_1}\frac{1-e^{-(\frac{d+0.5}{RC_1})T_s}}{(1-e^{\frac{dT_s}{RC_1}})(1-e^{\frac{0.5T_s}{RC_1}})}$	$\frac{1}{f_s}[\frac{1}{C_{eq}}-\sum_{i=1}^{m-1}\frac{e^{-\beta_i\pi/\omega_i}}{C_i(1+e^{-\beta_i\pi/\omega_i})}-\frac{e^{-\beta_0\pi/\omega_0}}{C_{eq}(1+e^{-\beta_0\pi/\omega_0})}]$	Single or Multi-Input SC Converters
CT modeling method [56]	Accurate Prediction and Design Guidelines	Output Capacitor Effect	$\frac{T_s}{2C_1}\coth(\frac{dT_s}{2RC_1})+\frac{(2C_o+C_1)^2T_s}{8C_1C_o(C_1+C_o)}+\frac{C_1R}{C_1+C_o}$	$\frac{T_s}{2C_{dis}}\coth(\frac{dT_s}{2R_{ch}C_{ch}})+\frac{(2C_o+C_{dis})^2T_s}{8C_{dis}C_o(C_{dis}+C_o)}+\frac{C_{dis}}{C_{dis}+C_o}R_{ch}$	Dual-Phase SC Converters without Complex Coupling Loops
CASBTC Modeling Method [57],[58]	Dynamic and Static States of SC Converters	Dynamical Operation States	$\frac{4R_LC(1-e^{-\frac{T_{on}}{RC}})}{(2R_LC-T_{on}-T_{off})(1-e^{\frac{T_{on}}{RC}})}*\frac{(1-e^{\frac{T_{off}}{RC}})}{(1-e^{\frac{T_{off}}{RC}})+2T_{off}(1-e^{\frac{T_{off}}{RC}})}$	$\frac{V_{c1max}+V_{c1min}+V_{c2max}+V_{c2min}}{2V_o}$	Dual-Phase SC Converters and Resonant SC Converters

[152]. It provides good performance in predicting the dynamic and static states of SC circuits. The dynamical states of input voltage, output voltage, the voltage of the flying capacitor, "ON time" of a transistor, "OFF time" of a transistor, or one switching cycle time are all included in the proposed model. This modeling method sets the charging time of the flying capacitor as the constant value. The output voltage could be regulated by adjusting the discharging time or one switching cycle time of the flying capacitor. If the "ON time" of a transistor is set less than the time constant τ of the charge loop, the operation range of an SC circuit could be largely expanded with the variable frequency control method.

In one switching cycle, the capacitor ampere-second balance of flying capacitor C could be derived as

$$Q_{\text{charge}} = I_{\text{ch}(t)}T_{\text{on}} = -Q_{\text{discharge}} = I_{\text{dis}(t)}T_{\text{off}} = I_{o(t)}T_{\text{off}} \tag{18}$$

where $I_{\text{ch}(t)}$ is the real-time charging current of the flying capacitor, $I_{\text{dis}(t)}$ is the real-time discharging current of the flying capacitor, T_{on} and T_{off} are the charging period and discharging period of the flying capacitor, and $I_{o(t)}$ is the real-time output current of the presented SC circuit in [57] and [58].

Considering the discharging period of T_{off} is linear, therefore, (18) could be rearranged as

$$\int_0^{T_{\text{on}}}\frac{V_{\text{in}}-I_{o(t)}\left(R_{\text{S1}}+r_d\right)-V_{C(t)}}{R_{\text{S1}}+r_d+r}dt = \left(\frac{\overline{V_{c1(t)}}+\overline{V_{c2(t)}}-V_{\text{o}}}{2r}\right)T_{\text{off}} \tag{19}$$

where $\overline{V_{c1(t)}}$ and $\overline{V_{c2(t)}}$ are the average voltage of the flying capacitors C_1 and C_2, respectively, in the T_{off} period.

The comparison of different modeling methods is given in Table III. According to Table III, most of the listed modeling methods have their own application limitations and may become inaccurate under certain operation conditions. Moreover, some modeling methods address the output filter capacitor effect on the steady-state behavior of SC circuits. The transient modeling method could predict the dynamical operation states by considering the real-time parameters of SC circuits. The different modeling methods will be suitable for the special SC circuits.

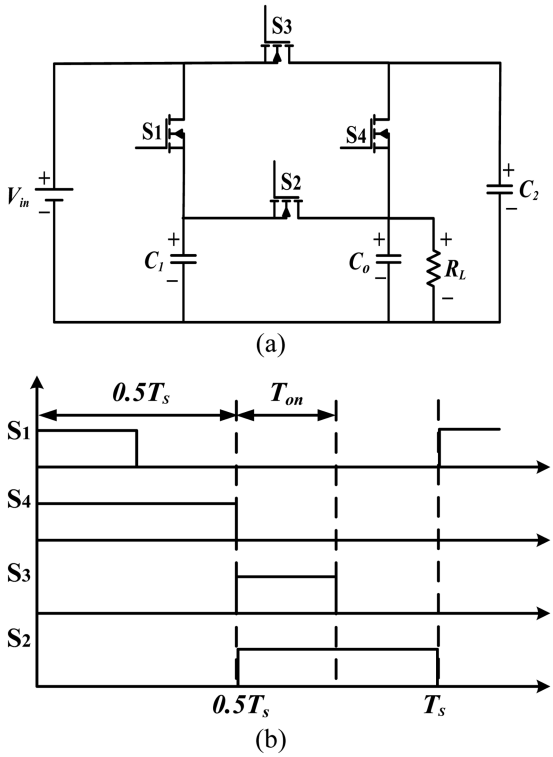

Fig. 6. Dual-phase step-down SC converter (a) circuit topology and (b) operation waveforms.

V. Control Methods for SC Circuits

SC circuit is a type of variable structure system. With the very fast charging and discharging speeds of capacitors, it is difficult to control the ON–OFF stages of the SC circuit to regulate the load voltage or load current. SC circuits are typically equipped with open-loop control or some linear feedback control methods. However, these approaches provide slow dynamic response speed, small operation regions, and large voltage ripples. Some new nonlinear control methods have been proposed in the literature to overcome these barriers to improve the power quality and extend the application area of SC circuits.

A. Pulsewidth Modulation Control Method for SC Circuit

There are different topologies of regulated SC circuits that adopt PWM control methods. In order to simplify the introduction of this control method, a basic dual-phase SC converter is presented in Fig. 6(a). Its driving waveforms of transistors are shown in Fig. 6(b). There are two operation states in one switching cycle. In the first half cycle, when switches S_1 and S_4 are ON and switches S_2 and S_3 are OFF, the flying capacitor C_1 is charged by the power source for T_{on} period. At the same period, flying capacitor C_2 discharges its stored energy to the load resistor and filter capacitor. During the period (T_{on}–$0.5T_s$), switch S_1 is turned OFF while switch S_4 is kept ON. As a result, flying capacitor C_2 continues discharging its stored energy to the load resistor and filter capacitor. As this dual-phase SC converter has a symmetrical topology, in the second half cycle, the roles of flying capacitors C_1 and C_2 are changed.

With the PWM control method [153], [154], [155], by changing the charging time of flying capacitor and keeping the constant discharging time ($0.5T_s$) with the constant frequency, a fixed SC converter structure could provide a wide range of output voltage from a given power source. Nevertheless, all these converters have the common drawback that spiky input currents with high EMI noise will occur. The switching devices will meet high current stress during the charging period of the flying capacitor.

B. Current Mode Control Method for SC Circuit

In order to solve the challenge of spiky input current in the regulated SC circuits with the PWM control method, a QSC converter is proposed in [156], [157], and [158] with the current control method. It features continuous input current and good regulation capability for SC converters. A dual-phase step-down QSC converter is built by connecting two basic QSC cells in parallel. It operates in an antiphase in each switching cycle. In this QSC converter, the charge quasi switches Q_{s1} and Q_{s3} are operated in the saturation region, acting as the voltage-controlled current source. The current magnitude is controlled by the gate–source voltage of the transistor ($V_{g,QS}$).

As shown in [156], [157], and [158], there are two operation stages in one switching cycle T_s. In the first-half switching cycle (0–$0.5T_s$), the flying capacitor C_1 is charged by the constant input current through the quasiswitch Q_{s1}. On the other hand, the flying capacitor C_2 discharges its energy to the load and filter capacitor through switch S_4. In the second-half switching cycle ($0.5T_s$–T_s), the roles of the flying capacitors C_1 and C_2 are changed. The duty time of all switches is fixed at $0.5T_s$, thus improving the regulation capability practically.

The conduction time for the charge switches in the PWM-controlled SC converter is short and the corresponding gate pulsewidth will be narrow at the light load or at low output voltage conditions. In order to keep the stable regulation of output voltage, the T_{on} time of the charge switches will be maintained with a much smaller value. However, such a PWM control method is hard to perform practically to implement with a very small T_{on} period. As shown in [147], compared with the PWM control method, with the current control scheme, the regulation for SC converters is improved as the voltage feedback control circuit is only required to provide a desired gate–source voltage to control the drain currents of quasiswitches with the fixed duty cycle 0.5.

C. Hysteretic Control Method for SC Circuit

A lower boundary hysteretic control method is proposed in [159]. It matches the output sampling frequency to the converter switching frequency across the entire load range; hence, the optimal output voltage ripple could be achieved. The presented converter achieves a peak efficiency of 86.40% and delivers a maximum output power of 5 mW. This article considers the SC converter changes phase N times in every M sampling period. N and M are integers, and $N \leq M$ since the frequency of phase change cannot exceed the sampling frequency. The output voltage is compared to the reference voltage once every sampling period, and the effective frequency of the converter's

phase change can be expressed as

$$f_{\text{ph\_change}} = \frac{N}{M} f_{\text{sample}} \tag{20}$$

$$NT_{\text{ph\_change}} = MT_{\text{sample}}. \tag{21}$$

The output voltage ripple is derived as

$$\Delta V_{\text{out,opt}} = \frac{\frac{M}{N} T_{\text{sample}} I_{\text{out}}}{C_{\text{fly}} + C_{\text{out}}} = \frac{I_{\text{out}}}{f_{\text{ph\_change}}(C_{\text{fly}} + C_{\text{out}})}. \tag{22}$$

The ratio between the bandwidth and the switching frequency should be set as

$$\frac{\omega_u}{\omega_{\text{sw}}} = \frac{\omega_u}{2\pi f_{\text{sw}}} = \frac{N_{\text{skip}} + 1}{\pi} I_{\text{CP}} t_d K_{vco} R_z \tag{23}$$

where N_{skip} is the number of skipped sampling pulses, K_{vco} is given as $K_{\text{vco}} = [(\partial f_{\text{sample}})/(\partial V_{\text{Control}})]$, and I_{CP} has the relationship with the average output current of integrator as $I_{\text{CP}} = \frac{t_{\text{CP}} f_{\text{sw}}}{I_{\text{avg}}}$.

D. Flying Capacitor Voltage Programmed Mode Control for SC Circuit

The authors in [160] proposed a flying capacitor voltage programmed mode control for SC circuits. Based on the steady-state operation analysis, this control method takes into account system dynamics and improves transient response by observing the flying capacitor voltage along with the output voltage. An inner control loop is built to regulate the output voltage to effectively reduce the order of the system. It allows us to achieve a faster transient response.

In this article, the current that flows through the flying capacitor is set as

$$I_{\text{fly}} = I_{\text{load}} \frac{C_{\text{fly}}}{C_{\text{fly}} + C_{\text{load}}}. \tag{24}$$

Considering the effect of allowing the SC circuits to operate at the lowest possible switching frequency for the given V_{ref}, the switching dynamics could be presented as

$$\dot{V}_{\text{fly}} = \begin{cases} f_1(x), & \text{if } g(x) < V_{\text{ref}} - \frac{V_{\text{in}}}{2} \\ f_s(x), & \text{if } V_{\text{ref}} - \frac{V_{\text{in}}}{2} < g(x) < \frac{V_{\text{in}}}{2} - V_{\text{ref}} \\ f_2(x), & \text{if } g(x) > \frac{V_{\text{in}}}{2} - V_{\text{ref}} \end{cases} \tag{25}$$

where $g(\text{x}) = V_{\text{fly}} - \frac{V_{\text{in}}}{2}$.

The functions $f_1(x)$ and $f_2(x)$ are derived from the state-space model as follows:

$$f_x = \begin{cases} f_1(x) = -\frac{V_{\text{fly}}}{2C_{\text{fly}}R_{\text{on}}} - \frac{V_{\text{out}}}{2C_{\text{fly}}R_{\text{on}}} + \frac{V_{\text{in}}}{2C_{\text{fly}}R_{\text{on}}} \\ f_2(x) = -\frac{V_{\text{fly}}}{2C_{\text{fly}}R_{\text{on}}} + \frac{V_{\text{out}}}{2C_{\text{fly}}R_{\text{on}}} \end{cases}. \tag{26}$$

The output voltage regulation is achieved by controlling the flying capacitor voltage to eliminate its dynamics. The output voltage could be regulated based on the equation of the reference voltage V_{ref}, the intermediate voltage $V_{\text{intermediate}}$, and the input voltage

$$V_{\text{intermediate}} = V_{\text{ref}} + \frac{C_{\text{load}}}{C_{\text{fly}} + C_{\text{load}}} (V_{\text{in}} - 2V_{\text{ref}}) \tag{27}$$

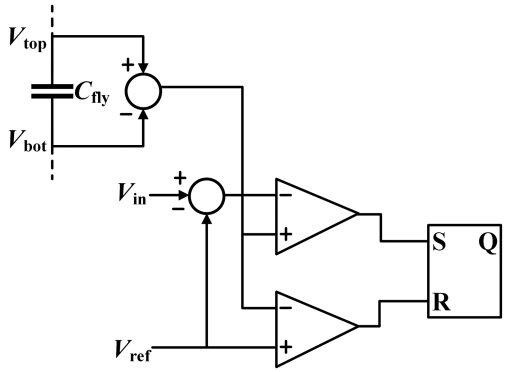

Fig. 7. Diagram of control through the steady-state voltage across the flying capacitor.

where $(V_{\text{in}} - 2V_{\text{ref}})$ is the difference between the input voltage and the voltage of the flying and output capacitors summed together at the moment of transition.

Assuming the time constants are smaller than the sensing delay, the maximum load current is approximately derived as

$$I_{\text{load max}} = \frac{C_{\text{fly}}(V_{\text{in}} - 2V_{\text{ref}})}{t_{\text{sense delay}}} \tag{28}$$

where $t_{\text{sense delay}} = \frac{1}{2f_{\max}}$, and $f_{\max}$ is the maximum switching frequency.

The control through the steady-state voltage across the flying capacitor is shown in Fig. 7.

E. Phase-Shift Control Method for SC Circuit

The authors in [161] and [162] presented the operating performance of an SC-based resonant converter using a phase-shift control method. The proposed phase-shift control method realizes ZVS operation, and thus achieves high-conversion efficiency. The average output current I_{out} could be expressed as

$$I_{\text{out}} = \frac{2V_{\text{in}}^2}{\omega_r^2 L_r T_{\text{sw}}} \times \frac{\sin \omega_r T_{pj} \sin \omega_r T_s'}{1 + \cos \omega_r T_s + \cos \omega_r T_s' + \cos \frac{\omega_r T_s}{2}} \tag{29}$$

where $T_s' = 0.5T_{\text{sw}} - |T_s|$.

The output voltage could be regulated by applying voltage feedback with PI gains. The reference of the averaged output current is given as follows:

$$I_{\text{out}}^*(s) = \left(K_p + \frac{K_i}{s}\right)[V_{\text{out}}^*(s) - V_{\text{ref}}(s)] \tag{30}$$

where K_{p} is the proportional gain, K_{i} is an integral gain, and $V_{\text{ref}}(s)$ is a reference of the output voltage.

The proposed feedback control achieved an accurate voltage regulation in spite of the input voltage fluctuation and voltage drops in devices.

The block diagram of the output voltage controller for the SC circuit is shown in Fig. 8.

The phase-shift control method is applied for SC circuits to achieve voltage regulation. However, the dead time and

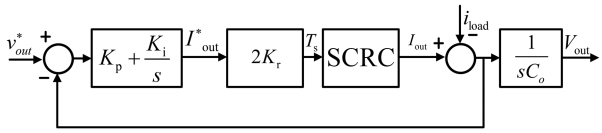

Fig. 8. Block diagram of the phase-shift controller.

parasitic parameters impose negative effects on the switching transit, resulting in a hard-switching process. It will cause extra switching loss. An optimized soft-switching method is proposed under phase-shift control in [161]. The transient analysis of resonance is analyzed based on the state trajectory. The influence of parasitic parameters on resonant current and output power is discussed. What is more, the dead time effect and soft-switching condition are taken into consideration.

Through the state trajectory and steady-state analysis, the output power is derived as

$$P_{\text{out}} = \frac{2MU_{\text{in}}^2}{\omega_r L_r T_s} \times \frac{\sin\omega_r T_{pj} \sin\omega_r(T_s/2 - T_{pj})}{1 + \cos\omega_r T_{pj} + \cos\omega_r(T_s/2 - T_{pj}) + \cos\frac{\omega_r T_s}{2}} \tag{31}$$

where T_{pj} is the phase-shift time, and $\omega_{\text{r}} = 2\pi f_{\text{r}}$.

The voltage conversion ratio was obtained as

$$M = \frac{2R_L}{\omega_r^2 L_r T_s} \times \frac{\sin\omega_r T_{pj} \sin\omega_r(T_s/2 - T_{pj})}{1 + \cos\omega_r T_{pj} + \cos\omega_r(T_s/2 - T_{pj}) + \cos\frac{\omega_r T_s}{2}}. \tag{32}$$

Sano and Fujita [162] proposed a phase shift plus PWM control strategy for SC circuits. With this control method, the output voltage regulation and the limitation of the loop peak current to a proper range are achieved. What is more, the output voltage ripple could be effectively reduced as well through the voltage ripple characteristics analysis in different cases.

With the proposed control method, the relationship between output voltage and the phase-shift angle could be derived as

$$V_{\text{out}} = \frac{2(1 + \frac{T}{RC}\cot^2(\frac{\pi-\theta}{2}))}{\frac{1}{2} + \frac{T}{RC}\cot^2(\frac{\pi-\theta}{2})} V_{\text{in}}. \tag{33}$$

F. Nonlinear Variable Structure Control (VSC) for SC Circuit

A nonlinear VSC method for dual-phase SC circuit, as shown in Fig. 6(a), is first shown in [163] and [164]. Based on the energy balance principle applied to the output capacitor, the instantaneous relationship of the output current and input current in charging and discharging periods is provided. The sliding mode switching functions are derived based on the VSC model.

A set of relationships describing the equivalent control signal of charge switch $\text{S}_1(U_{\text{s1}})$ was given as

$$\begin{cases} V_{C(S1)} = k[i_r + \frac{C_o}{\alpha_{\text{s1}}}(V_{\text{ref}} - v_o)] \\ \hat{v}_{\text{ramp(S1)}} = k\left[\frac{4(V_i - V_{c1})}{R_{\text{in}}}\right] \end{cases} \tag{34}$$

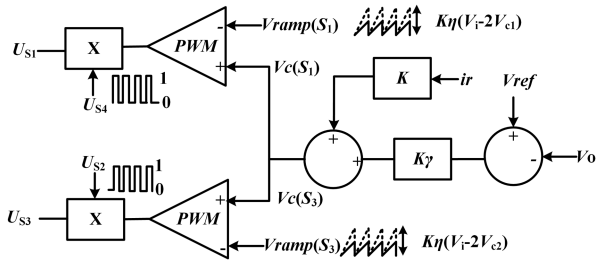

Fig. 9. Feedback circuit of the VSC method for a dual-phase SC circuit.

where $V_{C(S1)}$ is the feedback control signal for switch S_1, $\hat{v}_{\text{ramp(S1)}}$ is the peak magnitude of a constant frequency ramp signal, k is a down-scaling constant to adjust the signal level to an appropriate chip's level voltage standard, i_r is the load current, C_o is the capacitance of the filter capacitor, V_{ref} is the reference voltage, V_o is the output voltage, and V_i and V_{c1} are the input voltage and voltage of flying capacitor C_1, respectively; R_{in} is the equivalent resistance of the charge loop and α_{s1} represents the sliding coefficient.

A similar set of relationships describing the equivalent control signal of charge switch $\text{S}_3(U_{\text{s3}})$ is obtained as

$$\begin{cases} V_{C(S3)} = k\left[i_r + \frac{C_o}{\alpha_{\text{s3}}}(V_{\text{ref}} - v_o)\right] \\ \hat{v}_{\text{ramp(S3)}} = k\left[\frac{4(V_i - V_{c2})}{R_{\text{in}}}\right] \end{cases} \tag{35}$$

where $V_{C(S3)}$ is the feedback control signal for switch S_3, $\hat{v}_{\text{ramp(S3)}}$ is the peak magnitude of a constant frequency ramp signal, V_{c2} is the voltage of flying capacitor C_2, and α_{s3} represents the sliding coefficient.

Based on the relationships describing the equivalent control signals of charge switches $\text{S}_1(U_{\text{S1}})$ and $\text{S}_3(U_{\text{S3}})$, the feedback control mechanism of the nonlinear VSC method is shown in Fig. 9. This feedback circuit is similar to the conventional PWM voltage-mode controller but with additional feedback comments to detect the instantaneous load current for constructing the control signal V_{C}, input voltage V_i, and flying capacitors voltages V_{C1} and V_{C2} for controlling the ramp signals' amplitude. The nonlinear feedback control is achieved by these additional instantaneous sensors. As compared to the linear voltage feedback control approaches, much better transient response and steady-state regulation are provided with this control method in a wide operation range of input voltage and load. Under variable operation conditions, this control method is proven with a fast and robust performance of rejecting external disturbance.

The parameters of the feedback control mechanism using nonlinear variable structure control are $K = 0.1, \eta = 11.76$, and $\gamma = 2.2 + (14184.4)/(s)$ (the pole term in γ serves to reduce the steady-state error of the converter.)

G. Nonlinear Constant on Time Variable Frequency One-Cycle Control (CVFOCC) for SC Circuit

In combination with the dual-phase step-down SC circuit, as shown in Fig. 6, the voltage feedback circuit of the CVFOCC method in [165], [166], [167], and [168] is constructed, as shown in Fig. 10(a), and its operation waveform could be seen in

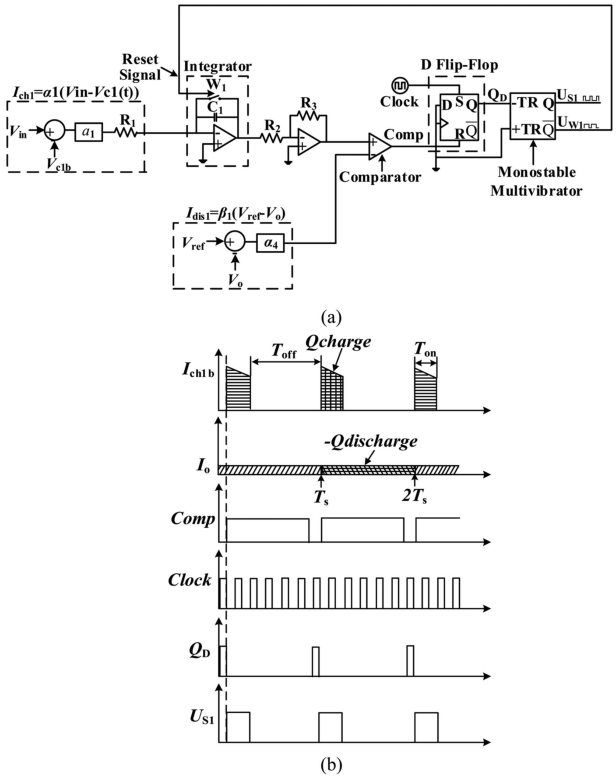

Fig. 10. Constant on time variable frequency one-cycle controller. (a) Control circuit. (b) Operation waveform of constant on time variable frequency one-cycle controller.

Fig. 10(b). Based on the dynamic ampere-second balance model and OCC method, the core control equation for this control method is derived as

$$Q_{\text{charge}} = \alpha_1 \int_0^{T_{\text{on}}} \left(V_{\text{in}} - V_{c1(t)}\right) dt = -Q_{\text{discharge}} = \beta_1 (V_{\text{ref}} - V_o)\, T_{\text{off}} \tag{36}$$

where V_{in} is the input voltage, $V_{c1(t)}$ is the instantaneous voltage of flying capacitor C_1, V_{ref} is the reference voltage, V_o is the output voltage, T_{on} is the "ON time" of switch S_1 and T_{off} is the "OFF time" of switch S_1, R_{in} is the equivalent resistance of charge loop of flying capacitor C_1, R_{dis} is the equivalent resistance of discharge loop of flying capacitor C_1, and α_1 and β_1 are the constant values.

For a dual-phase step-down SC circuit, as shown in Fig. 3(a), at the beginning of each switching cycle, the clock signal sets the D flip-flop high ($Q = 1, \overline{Q} = 0$) in Fig. 10. The monostable multivibrator will generate a constant pulsewidth square signal (constant T_{on} period) when the trailing edge of Q signal of D flip-flop arrives. The constant pulsewidth square signal will turn ON switch S_1 in Fig. 6(a) and turn OFF reset switch W_1 of the resettable integrator in Fig. 10(a). The charging current of C_1 ($I_{\text{ch1}(t)} = \alpha_1(V_{\text{in}} - V_{c1(t)})$) is integrated by the resettable integrator for constant T_{on} period. When T_{on} is over, the monostable multivibrator is reset low ($Q = 0, \overline{Q} = 1$). At this time point, the reset switch W_1 is turned ON and the resettable integrator

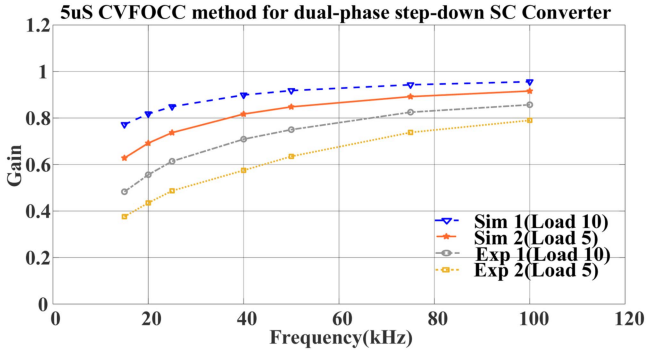

Fig. 11. Simulation and experimental results of CVFOCC method controlled 1X SC circuit with "constant on time" 5 μs.

TABLE IV
CVFOCC CONTROL UNIT PARAMETERS

"constant on time"	Integrator C_1	Pulsewidth of Monostable Multivibrator	Clock Signal of D flip-flop
5 μs	1μF	0.000005	Frquency:20 kHz Duty-cycle:0.2

in Fig. 6(a) is reset to zero. The switch in Fig. 6(a) will be concurrently turned ON by the control signal U_{s2}.

For T_{off} period, when the negative discharge of C_{1b} ($-Q_{\text{discharge}}$) reaches the charge of C_1 (Q_{charge}), the comparator in Fig. 7(a) will change its state from high to low. When the next clock signal arrives, the D flip-flop will be set high ($Q = 1$, $\overline{Q} = 0$) again. When the trailing edge of the Q signal of the D flip-flop arrives, the monostable multivibrator will then generate a constant pulsewidth signal for the new switching cycle. External disturbance can be rejected by adjusting the length of T_{off} period.

For the dual-phase step-down SC circuits, as shown in Fig. 6, the generation of control signal U_{s3} is similar to that of control signal U_{s1}. They share the same duty cycle yet with 180° phase shift as the reason for the phase shift of two clock signals. The control signals of $S_2(U_{s2})$ and $S_4(U_{s4})$ are 50% duty-cycle pulses complementing with each other and no regulation is required.

In the extension of this general control method to multistage symmetrical SC topologies, it is sufficient to consider only one of the phases when designing its feedback control loop. If this is achieved, the feedback control loops for the remaining phases could be easily performed following the same procedure.

A dual-phase step-down SC circuit, as shown in Fig. 6(a), is built to verify the dynamic ampere-second balance principle and the CVFOCC technique, as shown in [57] and [58]. Simulation results are achieved by the PSIM software. The simulation and experiment are conducted with the variable constant on time (5 μs) and load resistance (10 and 5 Ω). The comparison results are shown in Fig. 11. The control board parameters are given in Table IV.

The gain ratio will increase with the rise of the switching frequency. On the other hand, at the same frequency, the gain ratio will be lower at heavier loads. The maximum gain ratio is

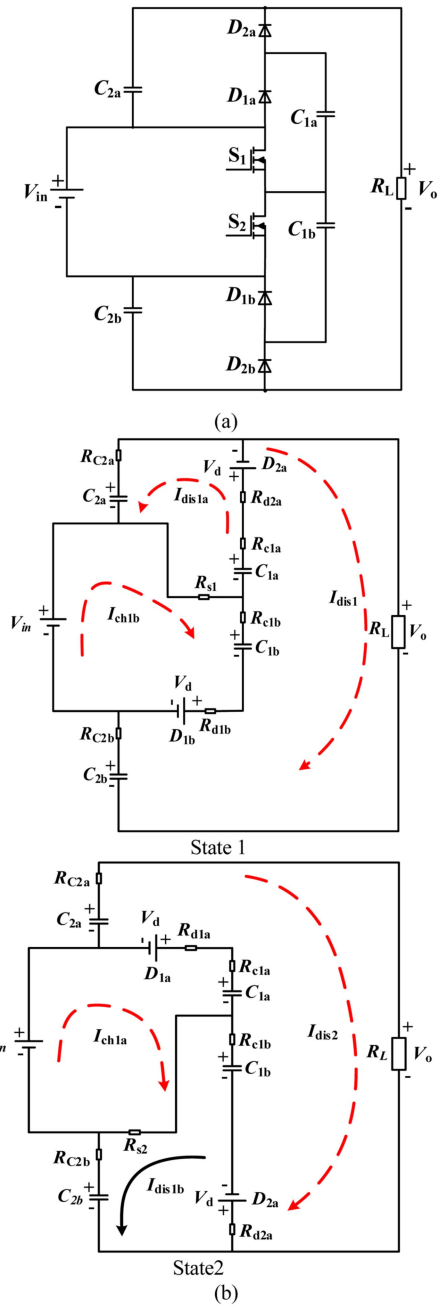

Fig. 12. (a) 3X TBSC converter topology. (b) Equivalent circuits of two operation states for the 3X TBSC converter.

close to 1 at the highest frequency. The simulation results have a good match with the experimental results. By controlling the switching frequency and maintaining the "constant on time," the output voltage regulation is achieved with the CVFOCC control method.

To verify that the CVFOCC technique is a general control method and the dynamical performance for the complex SC circuit, the simulation and experiment are also conducted on the 3X TBSC, as shown in Fig. 12(a). The operation waveforms can be seen in Fig. 12(b). The detailed operation principles and the dynamic ampere-second balance principle are shown in [57] and [58].

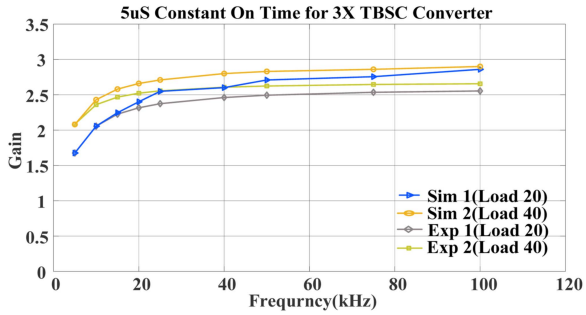

Fig. 13. Simulation and experimental results of the CVFOCC method controlled 3X TBSC converter with "constant on time" 5 μs.

Simulation is conducted with the variable constant on time (5 μs) and load resistance (20 and 40 Ω). Comparison results are shown in Fig. 13. Similar to the dual-phase step-down SC circuit, the gain ratio will increase with the rising switching frequency of the 3X TBSC converter. At a lighter load, this 3X TBSC converter will get a higher gain ratio at the same frequency. The maximum gain ratio for the CVFOCC-controlled 3X TBSC converter is close to 3 at the highest frequency. Simulation results also have a good match with the experimental results.

Therefore, the dynamic ampere-second balance principle and CVFOCC method are demonstrated with the general SC circuits. This control method is robust since the external disturbances can be instantaneously rejected by only adjusting the switching "OFF time." It has significantly improved the dynamic response speed in a wide operation range. Compared with other nonlinear control methods used for SC circuits, this control method is more straightforward and cost-effective with simpler control theory and analog circuits. The CVFOCC method is an extension of the OCC method [58] for general SC circuits. The OCC technique is adopted by incorporating the charge balance of the flying capacitor into the formulation of the OCC technique. The CVFOCC method delivers a robust and fast dynamical response speed for the operation of SC circuits. The switching frequency of SC circuits in the OCC control method purely depends on the state of the current switching cycle.

The dynamical response speed is also surveyed for the linear and nonlinear control methods in this article. Fig. 14 shows the simulated output voltage waveform of a 3X TBSC converter, which operates at an input voltage of 100 V. The load resistance alternates between 200 and 100 Ω [see Fig. 14(a) and (b)], CVFOCC method; Fig. 14(c) and (d), VSC method (with $k = 0.001$, and $\gamma = -5$); Fig. 14(e) and (f), PI control method; and Fig. 14(g) and (h), open-loop control wide input voltage and load operation range. Compared with the constant frequency control method that has the duty-cycle limitation (e.g., $0<d<0.5$), the different output power levels of variable frequency-controlled SC circuits could be achieved by only adjusting the switching frequency. Therefore, the operation range of SC circuits is enlarged with superior performances than the constant frequency control method. It will highly enlarge the application range of SC circuits.

In order to test the various output voltage regulation capabilities of different control methods with uniform standards,

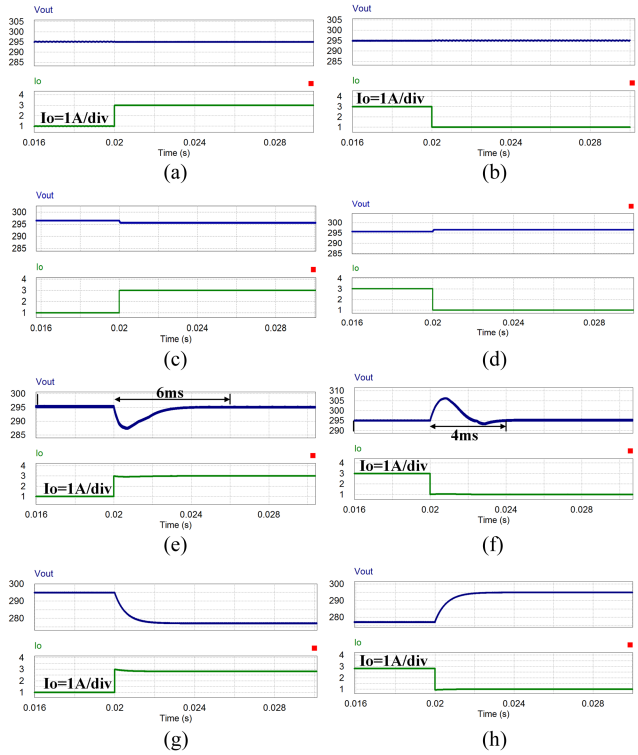

Fig. 14. Comparison of dynamical response speed for different control methods with 3X TBSC converter. (a) and (b) CVFOCC method. (c) and (d) VSC method. (e) and (f) PI control method. (g) and (h) Open-loop control method. (a) Io step-up, CVFOCC. (b) Io step-down, CVFOCC. (c) Io step-up, VSC. (d) Io step-down, VSC. (e) Io step-up, PI. (f) Io step-down, PI. (g) Io step-up, Open-loop. (h) Io step-down, Open-loop.

the target voltage is set as 295 V. Controlled by the open-loop control method, the output voltage is not maintained stable at the disturbance time point and 17 V voltage drop is observed, as shown in Fig. 14(g) and (h). In combination with the PI control method, as shown in Fig. 14(e) and (f), the response time to reject the disturbance in load current step-up and step-down is respectively 6 ms and 4 ms with 5 V voltage drop down or rise during the transient period. Compared to the aforementioned two control methods, the nonlinear control method could achieve a fast-dynamical response speed to deal with the load current step-up or step-down, as shown in Fig. 14(a)–(d). However, with the VSC method, the output voltage will have about 2 V voltage rise or drop down with the changeable load resistance, as shown Fig. 14(c) and (d). For the CVFOCC method, as shown in Fig. 14(a) and (b), the disturbance in load current is immediately rejected by changing the switching frequency with a nearly unnoticeable overshoot. Thus, the advantages of the nonlinear control technique in dynamic performance are demonstrated.

H. Comparison of Different Control Methods for SC Circuits

The comparison of control methods for the SC circuits is given in Table V. As given in Table V, the conventional control methods for SC converters, such as the PWM voltage feedback control method or the quasiswitch current mode control method, are the linear control methods. As a result, these control methods can be used in applications with normal precision of output voltage. SC circuits have more nonlinear characteristics (exponential charging and discharging operations) than conventional inductor-based converters. These linear control methods have good regulation performance on the inductor-based converters yet provide general line and load regulation in a narrow operation range on SC circuits. Based on the charge balance and the transient calculation modeling method, the nonlinear control methods such as the VSC control method and OCC method will exhibit good regulation and robust performances with fast dynamical response speed and low voltage ripples in a wide input voltage and load operation range.

VI. Technical Roadmap and Future Direction

SC circuits have been widely used for power conversion, power inversion, and power rectification for power supply. For low-power levels, they could be integrated into an IC circuit with high power density. For high-power applications, the small value inductors will be injected into the SC circuits to achieve the low current pulse and soft switching. Different modeling and control methods have been proposed to improve the quality of SC circuits. The technical roadmap and future direction of SC circuits are summarized.

A. Integration of SC Circuits

The fully integrated SC circuits are in great demand for implantable, wearable, and portable devices. The pure SC circuits could be integrated with the CMOS process design and BiCMOS process design. The fully integrated SC circuit technology is very challenging. The power efficiency of an SC circuit is not high enough over wide input and output voltage ranges. For an SC circuit, it has a finite output impedance, and its maximum deliverable power density is determined by the on-chip capacitance density. The increasing power density will always sacrifice power efficiency. As a result, in a standard CMOS process in which the capacitance density is low, there is a tradeoff between power density and efficiency, and optimizing this tradeoff could be very difficult [169], [170], [171]. The output voltage ripple hampers the performance of noise-sensitive devices. Lower voltage ripple requires higher switching frequency and larger capacitance. As a result, there is a balance between the output voltage ripple and the switching frequency. Hence, it is also a stringent problem to minimize voltage ripple using minimum system resources and cost.

For resonant SC circuits, more studies focus on structure optimization and control strategy, and the magnetic integrated design of the inductor of the converter is not yet mature. However, as an important part of the ReSC converter, inductors are the key factors that affect the quality and volume optimization of the converter. With the small value inductor, the integration of the resonant SC circuit is facing a challenging issue. At frequencies above 10 MHz, magnetic cores are typically impractical, and even with air-core magnetics, current crowding (skin and proximity) effects lead to high ac resistance [172]. The inductor is 1 mm^2 and uses 32 parallel traces with 11.5 μm width and 2.5 μm spacing. The design is fabricated in 130-nm RF silicon on

TABLE V
COMPARISON OF SURVEYED CONTROL METHODS FOR SC CIRCUITS

Control method	Control Type	Input Current	Control Algorithm	Response Speed	Operation Range	V_{out}
Open Loop	Linear	Spikey	/	/	Unlimited	/
PWM [155]	Linear	Spikey	$A_v(s)=\frac{(1+sC_a r_a)}{[sC_a r_a(1+sC_b r_b)]}$	Normal	Unlimited	$\begin{cases} v_o = Cx \\ x=[i_L v_{c1} v_{c1}]^T \end{cases}$
Current Mode [157]	Linear	Continue	$G_{OC}(s)=\frac{\hat{v}_{out}(s)}{\hat{v}_{GS}(s)}=\frac{K_2 R_L(1+C_o r_{C_o} s)}{1+\hat{\partial}_1 s+\hat{\partial}_0 s^2}$	Normal	Limited	$C_{av}(-A_{av}^{-1}B_{av})I_{ch}=R_L K_1(V_{GS}-V_T)^2$
Hysteretic Control Method [159]	Linear	Continue	$\frac{\omega_u}{\omega_{sw}}=\frac{\omega_u}{2\pi f_{sw}}=\frac{N_{skip}+1}{\pi} I_{CP} t_d K_{vco} R_z$	Normal	Limited	$f_{sw} C_{fly}(V_{in}-\Delta V_{cfly})$
Flying Capacitor Voltage Programmed Mode Control [160]	Linear	Continue	$V_{intermediate}=V_{ref}+\frac{C_{load}}{C_{fly}+C_{load}}(V_{in}-2V_{ref})$	Normal	Limited	$\frac{C_{fly}(V_{in}-2V_{ref})}{t_{sense\ delay}} R_{eq}$
Phase-shift Control Method [161],[162]	Linear	Continue	$I^*_{out}(s)=(K_p+\frac{K_i}{s})\left[V^*_{out}(s)-V_{ref}(s)\right]$	Normal	Limited	$\frac{2V_{in}^2}{\omega_t^2 L_t T_{sw}} * \frac{\sin\omega_t T_{pj} \sin\omega_t T_s'}{1+\cos\omega_t T_s+\cos\omega_t T_s'+\cos\frac{\omega_t T_s}{2}} R_{eq}$
VSC Method [163],[164]	Nonlinear	Spikey	$\begin{cases} V_{C(S1)}=k[i_r+\frac{C_o}{\alpha_{s1}}(V_{ref}-v_o)] \\ \hat{v}_{ramp(s1)}=k[\frac{4(V_i-V_{c1})}{R_{in}}] \end{cases}$	Fast	Limited	$\begin{cases} \frac{dv_{C1}}{dt}=\frac{v_o}{4r_L C_1}+\frac{C_o}{4C_1\alpha_{S1}}(V_{ref}-v_o)-\frac{(v_{C1}-v_o)}{2R_C C_1} \\ \frac{dv_{C3}}{dt}=\frac{v_o}{4r_L C_3}+\frac{C_o}{4C_3\alpha_{S3}}(V_{ref}-v_o)-\frac{(v_{C3}-v_o)}{2R_C C_3} \\ \frac{dv_o}{dt}=\frac{(v_{C1}-v_o)}{R_C C_o}+\frac{(v_{C3}-v_o)}{R_C C_o}-\frac{v_o}{r_L C_o} \end{cases}$
CVFOCC Method [165],[166] [167],[168]	Nonlinear	Soft	$\begin{aligned} Q_{charge}&=\alpha_1\int_0^{T_{on}}(V_{in}-V_{c1(t)})dt \\ &=-Q_{discharge}=\beta_1(V_{ref}-V_o)T_{off} \end{aligned}$	Fast	Unlimited	$\frac{4R_L C(1-e^{-\frac{T_{on}}{RC}})(1-e^{-\frac{T_{off}}{RC}})}{(2R_L C-T_{on}-T_{off})(1-e^{\frac{T_{on}}{RC}})(1-e^{\frac{T_{off}}{RC}})+2T_{off}(1-e^{\frac{T_{off}}{RC}})} V_{in}$

insulator (SOI) CMOS process with an active area of 5.5 mm^2. The authors in [173] proposed the fully integrated 400 V SC dc–dc converter. The topology exploits maximized dielectric energy storage at HV and significantly reduces the sidewall coupling of flying capacitors. It is implemented in 180-nm CMOS SOI technology. While it realizes a 33:1 conversion step, the measured power density is 119 mW/mm^2 at 63.60% efficiency. To solve the problem of decoupling caused by different resonant currents in the front and back of the circuit, magnetic integration design of high efficiency and high power density circuits has become a research hotspot.

To achieve the same resonant period before and after the resonant SC converter, it is necessary to ensure the consistency of inductance parameters. A decoupled magnetic integrated inductor without opening the air gap in the center column design has been proposed for the integration of a resonant SC converter [174], [175]. A 2–8 V V_{in} 670 mA scalable multiratio SC dc–dc converter for MCU integration in 28 nm CMOS achieving 91% peak efficiency, as shown in [175].

B. High Voltage Ratio Conversion of SC Circuits

The converters that adopt an SC structure have the advantage of HV gain. In these circuits, parallelized capacitors are charged by the power source. The capacitors are aligned in series and then release the stored energy to attain an HV gain. The HV conversion ratio dc–dc converter with HV gain ratio has become the main loop for the energy transfer of the renewable energy source or data center [176], [177], [178], [179].

Renewable energy systems powered by clean energy sources, such as PV and fuel cells (FC), have been warmly welcomed in recent years to provide part of the demanded energy of the local loads, dc microgrids, and ac grids. Unfortunately, the output voltage of these sources is usually lower than 50 V, and to meet the requirements of local loads and dc bus of single-phase inverters in ac grids, the output voltage of PV and FC should be boosted to around 400 V while it is about 800 V for a typical dc microgrids and three-phase inverter supplying the three-phase ac load or grid. Dealing with high-power levels, the interleaved structures are a promising solution due to the thermal distribution and minimized input current ripple. The isolated HV-gain quasiresonant dc–dc converter based on an SC circuit with bifunctional circuitry for renewable energy applications has been proposed with an HV gain ratio [180], [181]. The interleaved high step-up converter for renewable energy systems has been proposed by applying an SC mixed with a coupled inductor and built-in transformer voltage gain. The voltage stress could be adjusted by the turns' ratio of the coupled inductor and built-in transformer. It gives an extra degree of freedom [182].

The large and growing electricity consumption of modern data centers demands continuous improvement at the system level and converter levels. Due to the increase of output current, transient requirements, and power density, the two-stage power architecture is moving to lower input voltage at buck level. Therefore, higher step-down converters are required at the IBC level. At the system level, there are mainly two directions: conventional multistep conversions, e.g., from 48 to 12 V [183] or 48 to 6 V [184], and then 12 to 1 V, which normally achieve

higher efficiency but with more components and lower density. With data centers moving toward 48 V intermediate dc racks and the skyrocketing demands in automotive and telecommunication applications, high-ratio 48 to 1 V PoL power converters become one of the most popular topics in power IC and power electronics. The efficient and compact HSC converters are used for direct 48–1 V power conversion in data centers. The topology could be viewed as a 2-to-1 SC converter merged with two 8-to-1 series-capacitor-buck modules through two switching buses. Different from the conventional dc bus architecture, the switching bus architecture removes the bulky dc bus capacitors and reduces the number of switches with an HSC converter [185], [186].

C. Multilevel Conversion of SC Circuits

Different types of SC circuits have been the subject of research to fulfill the need for interconnecting renewable generation sources, existing or new grids, electronic loads, and battery-based systems. To deal with HV levels and high power, modular multilevel converter-based structures have been proposed. As they acted as the prosperous solution in developing ac–dc rectification, ac–ac conversion, dc–dc conversion, and dc–ac inversion for higher voltage and current ratio application, various structures have been presented where some of them could find their way into the power industrial market. SC circuits have been the subject of studies to be used in different applications where the power rating is higher than the usual for these types of converters or inverters. The scalability, capacitors voltage clamp, and the self-voltage balancing are the main features of these structures. However, the output voltage control limitations and the need to attenuate the current spikes are important drawbacks of SC circuits.

Due to their simple structures and self-voltage balancing characteristics, the HSC converter-based multilevel converters have been proposed with the output multilevel voltage advantages [187], [188]. The voltage static gain is independent of the number of submodules, allowing a good regulation range of the output voltage for HV applications. Moreover, the SC behavior provides an automatic clamp of the arms voltages, avoiding the need for ac loops to perform the arms voltage balance. The authors in [187] proposed a novel single dc-source SC compact multilevel topology based on packed E-Cell to have the boosting potency for the 11-level operation and to merit as a reliable ac–dc rectifier for fault-tolerant capability. A redundant switching states of flying capacitor-based multilevel converters are designed in [192] to balance the voltages of presented converters with the five-level power rectification capacity.

For SC circuits, the following challenges should be addressed to accelerate future development.

The first one is the integration of the control unit with the SC circuit. The system-level integration is an important part of the power supply for wearable, portable, or implanted devices. The fabricated HSC converter has been proposed, using a 180 nm BCD process, generating 0.8–1.8 V output from 12/24 V inputs with a 3 A maximum load. It achieves a peak power density of 355 mW/mm^3 with a power passive volume of 15.2 mm^3. It will bring the challenge for the control board integration [189].

The second one is the flexible features for flexible display devices or flexible screens for telephones, watches, and television. However, it is a big challenge for the design and manuscript of the bending capacitor and the bending transistors or diodes. Graphene materials are one of the options, as shown in [190].

The third one is the capacitance value of the flying capacitor (such as the electrolytic capacitor and ceramic capacitor) that will vary with switching frequency. As a result, voltage regulation or current regulation is not easily conducted with the linear control method, even with the nonlinear control method. For the charge balance principle, the charge and discharge of the flying capacitor should be balanced in one switching cycle. With the variable capacitance, the charge and discharge balances are difficult to maintain. The load voltage and current oscillation will be generated for the closed-loop control method and the open-loop control method. The thin-film capacitor has good capacitance stability characteristics. However, the price is high. It will highly raise the cost of the SC circuit.

The fourth one is the suitable control method. For SC circuits, the charging and discharging of a flying capacitor is very fast. The SC circuit has a nonlinear feature. Moreover, in combination with the inductors, the HSC converter and ReSC converter are of the second order or more systems. The related mathematical model is complex and not easy to build. Therefore, the regulation of the load voltage and the load current is more difficult than the inductor-based converter. What is more, for the high-quality SC circuit application, good load voltage or load current regulation performance such as the low-voltage ripples and the fast dynamical response speed should be provided with the nonlinear control method. However, the nonlinear control methods always have a complex control circuit. The control unit integration is even more difficult.

The fifth one is the service life of the capacitor in the case of frequent charge and discharge. Data on current failure rates of general power electronic equipment show that capacitor failure occupies 30% [191], [192]. The service life of capacitors is an increasing key design parameter in SC circuit power supplies. Power density demands are increasing, and the capacitors are the only component in the power supply that wears out. There are a number of key factors determining the expected service life of electrolytic capacitors used for SC circuits, such as the rated temperature, local heating effects, temperature derating, and magnitude and frequency of applied ripple currents. Fine design and technological manufacturing could improve the reliability and operation life of capacitors to meet operation requirements.

The sixth one is the limited high-power capacity. The HSC or resonant SC circuits have been used for high-power areas, such as EVs and renewable energy generation. Recently, for an ReSC converter, the 6000 W/in^3 power density at 48–12 V conversion and 80 A continuous output is achieved with the peak efficiency reaching 99.02%, and full-load efficiency reaching 97.67% [193]. However, the inductors should be injected in the charge loop, discharge loop, or both. As a result, the power density of SC circuits will be limited. The wide bandgap devices are adopted to improve the power density of SC circuits [194]. With the high switching frequency, the advanced drive circuit should be used for the special driving requirement for the wide

bandgap devices. The related control method suitable for the high switching frequency should be proposed and designed. In future work, the equivalent inductor of capacitors and equivalent inductor of the charge and discharge loop could be used to act as the equivalent inductor to build a resonant *LC* circuit to achieve ZVS and ZCS functions. It could be adopted for different power-level applications.

The seventh one is the high charging current for SC circuits. The nonlinear characteristics of SC circuits bring challenges to the controller design. For an SC circuit, the time constant τ of the charge loop is typically small. The high charging current will occur ($i = \Delta Q_{\mathrm{C}}/T_{\mathrm{S}}$). To achieve effective regulation, it is necessary for a controller to ensure the turn-ON time of a transistor below the time constant τ of the charging loop. In order to achieve the soft charging current, the dead time is added to extend the charging period and discharging period. The small value inductor is also injected in the charge loop and discharge loop of the flying capacitor. However, the low frequency and the additional inductor will limit the high integration of the SC circuit. The nonlinear variable frequency control method and the self-equivalent inductance and resistance of the SC circuit could be utilized to solve this issue.

VII. Conclusion and Discussions

For the high power density, none or less magnetic components, and high integration capacity, SC circuits have been widely used and deeply studied for many years. This article presents a review of different topologies, application areas, modeling methods, and control methods for SC circuits. The topologies of SC circuits have been classified and compared in this article. The application areas of SC circuits are presented and summarized. The steady-state modeling method, transient modeling method, average current modeling, and so on are all presented in this article. The different features of the modeling methods are surveyed. The linear and nonlinear control methods are presented in this article. A comparison of different control methods is conducted. The theory and feedback circuits of different control methods are derived. As the nonlinear features of SC circuits, the nonlinear control methods provide better performances on dynamical response speed, voltage ripple, and load regulation in a wider operation range than the traditional linear control methods. The technical roadmap and future direction are concluded for the future development of SC circuits. The challenges should be addressed for SC circuits and are also summarized in this article. This article provides guidance for the selection, simulation, and voltage regulation of SC circuits. It could be used as a reference for design and theory analysis for SC circuits.

References

[1] Q. Lu, S. Li, B. Zhao, J. Jiang, Z. Chen, and S. Du, "A dynamically reconfigurable recursive switched- capacitor DC–DC converter with adaptive load ability enhancement," *IEEE Trans. Power Electron.*, vol. 38, no. 4, pp. 5032–5040, Apr. 2023.

[2] D.-H. Park and R.-Y. Kim, "Accelerated model predictive control based on a greedy algorithm with round-robin priority for N-level single-phase flying capacitor converter in solid-state transformer," *IEEE Trans. Ind. Electron.*, vol. 70, no. 7, pp. 6735–6743, Jul. 2023.

[3] Z. Xia and J. T. Stauth, "Constant switch stress control of hybrid switched capacitor DC-DC converters," in *Proc. IEEE Appl. Power Electron. Conf. Expo.*, 2022, pp. 1214–1221.

[4] C. Rech and W. A. P. Castiblanco, "Five-level switched-capacitor ANPC inverter with output voltage boosting capability," *IEEE Trans. Ind. Electron.*, vol. 70, no. 1, pp. 29–38, Jan. 2023.

[5] D. Hulea, M. Gireadă, O. Cornea, and N. Muntean, "An improved bidirectional hybrid switched capacitor converter," in *Proc. IECON 48th Annu. Conf. IEEE Ind. Electron. Soc.*, 2022, pp. 1–6.

[6] Y. Zhong, W.-H. Ki, and J. Jiang, "Fully-integrated switched-capacitor converter with capacitor bridging for improved current density," *IEEE Trans. Circuits Syst. II, Exp. Briefs*, vol. 69, no. 10, pp. 4063–4067, Oct. 2022.

[7] A. Dago, M. Leoncini, S. Saggini, S. Levantino, and M. Ghioni, "Hybrid resonant switched-capacitor converter for 48–3.4V direct conversion," *IEEE Trans. Power Electron.*, vol. 37, no. 11, pp. 12998–13002, Nov. 2022.

[8] W. Xie and K. M. Smedley, "Seven switching techniques for the ladder resonant switched-capacitor converters with full-range voltage regulation," *IEEE Trans. Ind. Electron.*, vol. 69, no. 8, pp. 7897–7908, Aug. 2022.

[9] X. Zheng and P. Luo, "A fully integrated switched capacitor power converter with minimum driving loss point tracking technique," *IEEE Trans. Circuits Syst. II, Exp. Briefs*, vol. 69, no. 12, pp. 4959–4963, Dec. 2022.

[10] A. Jackson, N. M. Ellis, and R. C. N. Pilawa-Podgurski, "A capacitively-isolated dual extended LC-tank hybrid switched-capacitor converter," in *Proc. IEEE Appl. Power Electron. Conf. Expo.*, 2022, pp. 1279–1283.

[11] S. Han, Y. Wang, Z. Xie, Y. Guan, J. M. Alonso, and D. Xu, "Continuously adjustable modular bidirectional switched-capacitor DC–DC converter," *IEEE Trans. Power Electron.*, vol. 37, no. 11, pp. 12944–12948, Nov. 2022.

[12] J. Qi et al., "A multiple-modes resonant switched capacitor DC/DC converter with variable voltage ratios," *IEEE Trans. Power Electron.*, vol. 38, no. 6, pp. 7428–7443, Jun. 2023.

[13] H. Lei, R. Hao, X. You, F. Li, and M. Zhou, "Nonisolated high step-up soft-switching DC-DC converter integrating Dickson switched-capacitor techniques," in *Proc. IEEE Energy Convers. Congr. Expo.*, 2018, pp. 1247–1252.

[14] S. Li, Z. Li, W. Shang, S. Zheng, and P. Jia, "A family of hybrid step-up DC-DC converters based on switched-capacitor converters," in *Proc. IEEE 9th Int. Power Electron. Motion Control Conf.*, 2020, pp. 497–502.

[15] K. K. Law, K. W. E. Cheng, and Y. P. B. Yeung, "Design and analysis of switched-capacitor-based step-up resonant converters," *IEEE Trans. Circuits Syst. I, Regular Papers*, vol. 52, no. 5, pp. 943–948, May 2005.

[16] W. Xie et al., "A step-up series-parallel resonant switched-capacitor converter with extended line regulation range," in *Proc. IEEE Appl. Power Electron. Conf. Expo.*, 2019, pp. 2150–2154.

[17] G. Marin, J. Kim, J.-M. Seo, and A. Neviani, "A 13.56 MHz reconfigurable step-up switched capacitor converter for wireless power transfer system in implantable medical devices," in *Proc. IEEE Wireless Power Transfer Conf.*, 2020, pp. 361–364.

[18] M. Zanwar and S. Sen, "Design of CMOS programmable output binary and fibonacci switched capacitor step-down DC-DC converter," in *Proc. Int. Conf. Very Large Scale Integr. Syst., Architectures, Technol. Appl.*, 2016, pp. 1–6.

[19] J. Qi, X. Wu, Y. Zhao, and J. Liu, "High step-down ZCS buck converter with switched capacitor," in *Proc. IEEE Energy Convers. Congr. Expo.*, 2020, pp. 924–929.

[20] Q. Wang, P. Yang, H. Jiang, Y. Guo, W. Jia, and Z. Wang, "A 34 nA quiescent current switched-capacitor step-down converter with 1.2V output voltage and 0–5μA load current," in *Proc. IEEE Int. Symp. Circuits Syst.*, 2020, pp. 1–5.

[21] L. Yu, L. Wang, W. Mu, and C. Yang, "An ultrahigh step-down DC–DC converter based on switched-capacitor and coupled inductor techniques," *IEEE Trans. Ind. Electron.*, vol. 69, no. 11, pp. 11221–11230, Nov. 2022.

[22] R. Marusarz, "A switched capacitor, inductor less DC to AC voltage step-up power converter," in *Proc. 20th Annu. IEEE Power Electron. Spec. Conf.*, 1989, pp. 99–103.

[23] D. F. Cortez and I. Barbi, "A three-phase multilevel hybrid switched-capacitor PWM PFC rectifier for high-voltage-gain applications," *IEEE Trans. Power Electron.*, vol. 31, no. 5, pp. 3495–3505, May 2016.

[24] J. Liu, L. Li, P. Chen, W. He, Y. Wang, and Q. Ding, "Research on symmetrical switched capacitor multilevel AC-AC converter," in *Proc. IEEE 16th Conf. Ind. Electron. Appl.*, 2021, pp. 912–915.

[25] L. Müller and J. W. Kimball, "A dynamic model of switched-capacitor power converters," *IEEE Trans. Power Electron.*, vol. 29, no. 4, pp. 1862–1869, Apr. 2014.

[26] J. W. Kimball, "Performance analysis of generalized algebraic switched capacitor converters," in *Proc. IEEE Energy Convers. Congr. Expo.*, 2013, pp. 1808–1813.

[27] H. Kim, C. Park, and C. Kim, "An output-boosted 3-ratio switched-capacitor DC-DC converter with 0.5-to-1.8 V output voltage range for low-power IoT applications," in *Proc. IEEE 65th Int. Midwest Symp. Circuits Syst.*, 2022, pp. 1–4.

[28] Y. Lu, J. Jiang, and W.-H. Ki, "Design considerations of distributed and centralized switched-capacitor converters for power supply on-chip," *IEEE J. Emerg. Sel. Topics Power Electron.*, vol. 6, no. 2, pp. 515–525, Jun. 2018.

[29] S. Kanzaki, T. Hirose, H. Asano, Y. Nakazawa, N. Kuroki, and M. Numa, "Switched-capacitor voltage buck converter with step-down-ratio and clock-frequency controllers for ultra-low-power IoT devices," in *Proc. 25th IEEE Int. Conf. Electron., Circuits Syst.*, 2018, pp. 209–212.

[30] S. M. Ahsanuzzaman, A. Prodić, and D. A. Johns, "An integrated high-density power management solution for portable applications based on a multioutput switched-capacitor circuit," *IEEE Trans. Power Electron.*, vol. 31, no. 6, pp. 4305–4323, Jun. 2016.

[31] B. Maity and P. Mandal, "A high performance switched capacitor-based DC-DC buck converter suitable for embedded power management applications," *IEEE Trans. Very Large Scale Integr. Syst.*, vol. 20, no. 10, pp. 1880–1885, Oct. 2012.

[32] Y.-C. Lin, Y.-K. Luo, K.-H. Chen, and W.-C. Hsu, "Liquid crystal display (LCD) supplied by highly integrated dual-side dual-output switched-capacitor DC-DC converter with only two flying capacitors," *IEEE Trans. Circuits Syst. I, Regular Papers*, vol. 59, no. 2, pp. 439–446, Feb. 2012.

[33] J. Huang, Z. Tong, Y. Lu, C.-S. Lam, and R. P. Martins, "A 5V-to-0.5V inductor-first inductor-on-ground switched capacitor multi-path hybrid DC-DC converter," in *Proc. IEEE Custom Integr. Circuits Conf.*, 2023, pp. 1–2.

[34] E. Voulgari, F. Krummenacher, and M. Kayal, "Design of an energy-efficient current-to-frequency converter for a wearable sensor platform," in *Proc. 26th Int. Conf. Mixed Des. Integr. Circuits Syst.*, 2019, pp. 210–214.

[35] S.-Y. Lin et al., "A multi-phase series-parallel with bond wire auxiliary fully-integrated 250 pF switched-capacitor with 13.6 mV output ripple for supplying temperature sensor with 0.1 °C accuracy to early detect COVID-19," in *Proc. IEEE Asian Solid-State Circuits Conf.*, 2021, pp. 1–3.

[36] J. Jiang, Y. Lu, C. Huang, W.-H. Ki, and P. K. T. Mok, "20.5 A 2-/3-phase fully integrated switched-capacitor DC-DC converter in bulk CMOS for energy-efficient digital circuits with 14% efficiency improvement," in *Proc. IEEE Int. Solid-State Circuits Conf. Dig. Tech. Papers*, 2015, pp. 1–3.

[37] Y. Lu, J. Jiang, and W.-H. Ki, "A multiphase switched-capacitor DC–DC converter ring with fast transient response and small ripple," *IEEE J. Solid-State Circuits*, vol. 52, no. 2, pp. 579–591, Feb. 2017.

[38] G. Cai, Y. Lu, and R. Martins, "A battery-input sub-1V output 92.9% peak efficiency 0.3A/mm2 current density hybrid SC-parallel-inductor buck converter with reduced inductor current in 65nm CMOS," in *Proc. IEEE Int. Solid- State Circuits Conf.*, 2022, pp. 312–314.

[39] Z. Ye, S. R. Sanders, and R. C. N. Pilawa-Podgurski, "Modeling and comparison of passive component volume of hybrid resonant switched-capacitor converters," *IEEE Trans. Power Electron.*, vol. 37, no. 9, pp. 10903–10919, Sep. 2022.

[40] W. Chen, A. Huang, C. Li, and G. Wang, "A high efficiency high power step-up resonant switched-capacitor converter for offshore wind energy systems," in *Proc. IEEE Energy Convers. Congr. Expo.*, 2012, pp. 235–239.

[41] H. Shojaeian, S. Hasanzadeh, and S. M. Salehi, "A single switch high voltage gain DC-DC converter based on coupled inductor and switched-capacitor for renewable energy systems," in *Proc. 12th Power Electron., Drive Syst., Technol. Conf.*, 2021, pp. 1–6.

[42] F. Zhang, L. Du, F. Z. Peng, and Z. Qian, "A new design method for high-power high-efficiency switched-capacitor DC–DC converters," *IEEE Trans. Power Electron.*, vol. 23, no. 2, pp. 832–840, Mar. 2008.

[43] A. Kawa, R. Stala, A. Mondzik, S. Pirog, and A. Penczek, "High-power thyristor-based DC–DC switched-capacitor voltage multipliers: Basic concept and novel derived topology with reduced number of switches," *IEEE Trans. Power Electron.*, vol. 31, no. 10, pp. 6797–6813, Oct. 2016.

[44] S. Liu, Q. Dong, Y. Fu, S. Li, and G. Zhang, "A family of high step-up isolated DC-DC converters based on Fibonacci switched-capacitor cell," in *Proc. Int. Power Electron. Conf. Energy Convers. Conf. Expo Asia*, 2022, pp. 2641–2646.

[45] S. Ren et al., "Cascaded resonant switched capacitor auxiliary power supply for medium voltage DC," in *Proc. IEEE Appl. Power Electron. Conf. Expo.*, 2022, pp. 430–435.

[46] Y. Liu, X. Yang, Y. Wang, H. Tan, T. Q. Zheng, and S. Igarashi, "Isolated resonant switched capacitor converter with voltage self-balancing ability," *IEEE Trans. Transp. Electrific.*, vol. 8, no. 3, pp. 3921–3933, Sep. 2022.

[47] M. Uno, T. Sanada, and Y. Fujii, "Analysis and theoretical comparison of 1-to-1.5 resonant switched capacitor converters for high-voltage EV batteries," in *Proc. Int. Power Electron. Conf. Energy Convers. Conf. Expo Asia*, 2022, pp. 2312–2319.

[48] M. Krstic, M. Pahlevani, S. Eren, and P. Jain, "Averaged, curvature-based model of switched-capacitor converters," in *Proc. IEEE Appl. Power Electron. Conf. Expo.*, 2019, pp. 2859–2864.

[49] M. Muhammad, M. Armstrong, and M. A. Elgendy, "Modeling and control of non-isolated high voltage gain boost converter employing coupled inductor and switched capacitor," in *Proc. Int. Conf. Students Appl. Eng.*, 2016, pp. 312–317.

[50] Y.-H. Chang and Y.-J. Chen, "Modeling and implementation of high-gain switched-inductor switched-capacitor converter," in *Proc. Int. Symp. Integr. Circuits*, 2014, pp. 9–12.

[51] Y. Ye and K. W. E. Cheng, "Voltage-gap modeling method for single-stage switched-capacitor converters," *IEEE J. Emerg. Sel. Topics Power Electron.*, vol. 2, no. 4, pp. 808–813, Dec. 2014.

[52] S. Ben-Yaakov, "Behavioral average modeling and equivalent circuit simulation of switched capacitors converters," *IEEE Trans. Power Electron.*, vol. 27, no. 2, pp. 632–636, Feb. 2012.

[53] S. Khatua, D. Kastha, and S. Kapat, "Exact-order discrete-time modeling of a DAB derived hybrid switched-capacitor converter," in *Proc. IEEE Appl. Power Electron. Conf. Expo.*, 2022, pp. 2051–2057.

[54] D. Li, G. Roberts, and A. Prodić, "Exponential flying capacitor converter," in *Proc. IEEE 23rd Workshop Control Model. Power Electron.*, 2022, pp. 1–6.

[55] R. Middlebrook and S. Cuk, "A general unified approach to modeling switching-converter power stages," in *Proc. IEEE Power Electron. Spec. Conf.*, 1976, pp. 18–34.

[56] B. Wu, L. Wang, L. Yang, K. M. Smedley, and S. Singer, "Comparative analysis of steady-state models for a switched capacitor converter," *IEEE Trans. Power Electron.*, vol. 32, no. 2, pp. 1186–1197, Feb. 2017.

[57] L. Yang, B. Wu, X. Tong, K. M. Smedley, and G.-P. Li, "Dynamic capacitor ampere-second balance transient calculation modeling method for switched-capacitor converters," *IEEE Trans. Power Electron.*, vol. 33, no. 10, pp. 8916–8926, Oct. 2018.

[58] B. Wu, L. Yang, X. Zhang, K. M. Smedley, and G.-P. Li, "Modeling and analysis of variable frequency one-cycle control on high-power switched-capacitor converters," *IEEE Trans. Power Electron.*, vol. 33, no. 6, pp. 5465–5475, Jun. 2018.

[59] L.-L. Wang, Y.-F. Zhou, and J.-N. Chen, "Study on the dynamical model and analytical method for DC-DC switching converter," in *Proc. CES/IEEE 5th Int. Power Electron. Motion Control Conf.*, 2006, pp. 1–5.

[60] L. Schmitz, D. C. Martins, and R. F. Coelho, "Generalized high stepup DC-DC boost-based converter with gain cell," *IEEE Trans. Circuits Syst. I, Regular Papers*, vol. 64, no. 2, pp. 480–493, Feb. 2017.

[61] Q. Zhao and F. C. Lee, "High-efficient, high step-up DC-DC converters," *IEEE Trans. Power Electron.*, vol. 18, no. 1, pp. 65–73, Jan. 2003.

[62] A. Ayachit and M. K. Kazimierczuk, "Averaged small-signal model of PWM DC-DC converters in CCM including switching power loss," *IEEE Trans. Circuits Syst. II, Exp. Briefs*, vol. 66, no. 2, pp. 262–266, Feb. 2019.

[63] A. F. Witulski, "Introduction to modeling of transformers and coupled inductors," *IEEE Trans. Power Electron.*, vol. 10, no. 3, pp. 349–357, May 1995.

[64] S. Hasanpour, A. Baghramian, and H. Mojallali, "Reduced-order small signal modeling of high-order high step-up converters with clamp circuit and voltage multiplier cell," *Int. Eng. Technol. Power Electron.*, vol. 12, no. 13, pp. 3539–3554, Nov. 2019.

[65] M. Forouzesh, Y. P. Siwakoti, F. Blaabjerg, and S. Hasanpour, "Small signal modeling and comprehensive analysis of magnetically coupled impedance-source converters," *IEEE Trans. Power Electron.*, vol. 31, no. 11, pp. 7621–7641, Nov. 2016.

[66] M. Das and V. Agarwal, "Generalized small signal modeling of coupled-inductor-based high-gain high-efficiency DC-DC converters," *IEEE Trans. Ind. Appl.*, vol. 53, no. 3, pp. 2257–2270, May/Jun. 2017.

[67] L. Schmitz, D. C. Martins, and R. F. Coelho, "A simple, accurate small-signal model of a coupled-inductor-based DC-DC converter including the leakage inductance effect," *IEEE Trans. Circuits Syst. II, Exp. Briefs*, vol. 68, no. 7, pp. 2533–2537, Jul. 2021.

[68] L. Müller and J. W. Kimball, "Effects of stray inductance on hard-switched switched capacitor converters," *IEEE Trans. Power Electron.*, vol. 29, no. 12, pp. 6276–6280, Dec. 2014.

[69] H. Tan, X. Yang, Y. Liu, C. Yan, T. Q. Zheng, and Q. Chen, "Comparison of short-circuit current control of resonant switched-capacitor converter," in *Proc. IEEE Transp. Electrific. Conf. Expo*, 2022, pp. 1272–1277.

[70] P. Majumder, S. Kapat, and D. Kastha, "Fast transient state feedback digital current mode control design in series capacitor buck converters," in *Proc. IEEE Appl. Power Electron. Conf. Expo.*, 2022, pp. 2080–2085.

[71] A. K. Upadhiya, L. N, and M. K. Mishra, "A common ground switched-capacitor high gain boost converter for wide voltage regulation," in *Proc. IEEE Int. Conf. Power Electron., Smart Grid, Renewable Energy*, 2022, pp. 1–6.

[72] L. He and X. Xu, "Soft-switching bidirectional switched-capacitor DC–DC converter with multiple phase shift control methods," *IEEE J. Emerg. Sel. Topics Power Electron.*, vol. 10, no. 2, pp. 1537–1547, Apr. 2022.

[73] X. Lin, R. Burgos, and D. Dong, "Improved variable switching frequency control for capacitor voltage ripple regulation in multilevel flying capacitor converter," *IEEE Trans. Power Electron.*, vol. 38, no. 5, pp. 5700–5705, May 2023.

[74] B. Wang, R. Burgos, and B. Wen, "An average model for three-phase five-level flying capacitor converters with phase-shifted PWM," in *Proc. IEEE Energy Convers. Congr. Expo.*, 2022, pp. 1–8.

[75] W. Ma, B. Zhang, and D. Qiu, "Robust single-loop control strategy for four-level flying-capacitor converter based on switched system theory," *IEEE Trans. Ind. Electron.*, vol. 70, no. 8, pp. 7832–7844, Aug. 2023.

[76] Y. Zeng, H. Li, H. Du, Z. Qiu, and Z. Chen, "A single-switch capacitor clamped non-resonant linear soft-switching DC-DC converter," in *Proc. IEEE Energy Convers. Congr. Expo.*, 2021, pp. 1757–1761.

[77] X. Ding, F. Wang, M. Zhou, Y. Cao, and Z. We, "Soft switching high voltage gain quasi-Z-source DC–DC converter with switched-capacitor technique," *IEEE Trans. Ind. Electron.*, vol. 69, no. 11, pp. 11231–11241, Nov. 2022.

[78] E. Hamo, M. Evzelman, and M. M. Peretz, "Modeling and analysis of resonant switched-capacitor converters with free-wheeling ZCS," *IEEE Trans. Power Electron.*, vol. 30, no. 9, pp. 4952–4959, Sep. 2015.

[79] P. S. Dash and S. P. Das, "An enhanced soft charging switched-capacitor multi-level inverter for HFAC applications," in *Proc. IEEE Glob. Conf. Comput., Power Commun. Technol.*, 2022, pp. 1–4.

[80] A. Wei, B. Lehman, W. Bowhers, and M. Amirabadi, "A soft-switching non-inverting buck-boost converter," in *Proc. IEEE Appl. Power Electron. Conf. Expo.*, 2021, pp. 1920–1926.

[81] M. R. A. Siddique, M. J. Ferdous, and I. Islam, "Switched capacitor based soft-switching DC-DC boost converter for high voltage gain," in *Proc. 8th Int. Conf. Elect. Comput. Eng.*, 2014, pp. 820–823.

[82] S. Li, S. Liang, Z. Li, and S. Zheng, "A phase-shift-modulated resonant two-switch boosting switched-capacitor converter and its modulation map," *IEEE Trans. Ind. Electron.*, vol. 70, no. 8, pp. 7783–7795, Aug. 2023.

[83] R. Kopacz, M. Harasimczuk, P. Trochimiuk, and J. Rąbkowski, "Investigation of soft-switching QSW technique in DC/DC SiC-based flying capacitor converter with Q2L control," *IEEE Trans. Ind. Electron.*, vol. 70, no. 9, pp. 9035–9045, Sep. 2023.

[84] P. Wang, R. Ling, and D. Li, "A state trajectory control method for switched-capacitor-based resonant converter with the finite state machine controller," in *Proc. IEEE Energy Convers. Congr. Expo.*, 2021, pp. 2971–2978.

[85] V. R. Vakacharla, A. K. Rathore, R. K. Singh, and S. K. Mishra, "Fixed-frequency current-fed LCL series resonant soft-switching converter with capacitive doubler," *IEEE Trans. Ind. Appl.*, vol. 57, no. 6, pp. 6611–6621, Nov./Dec. 2021.

[86] S. V. Cheong, H. Chung, and A. Ioinovici, "Inductor less DC-to-DC converter with high power density," *IEEE Trans. Ind. Electron.*, vol. 41, no. 2, pp. 208–215, Apr. 1994.

[87] T. Umeno, K. Takahashi, I. Oota, F. Ueno, and T. Inoue, "New switched-capacitor DC-DC converter with low input current ripple and its hybridization," in *Proc. 33rd Midwest Symp. Circuits Syst.*, 1990, pp. 1091–1094.

[88] L. Oota, T. Inoue, and F. Ueno, "A realization of low-power supplies using switched-capacitor transformers and its analysis," *Trans. Inst. Electron. Commun. Eng. Jpn.*, vol. J66-C, no. 8, pp. 576–583, Aug. 1983.

[89] F. Ueno, T. Inoue, I. Oota, and I. Harada, "Emergency power supply for small computer systems," in *Proc. IEEE Int. Symp. Circuits Syst.*, 1991, pp. 1065–1068.

[90] R. D. Middlebrook, "Transformerless DC-to-DC converters with large conversion ratios," in *Proc. Int. Telecommun. Energy Conf.*, 1984, pp. 455–460.

[91] B. Wu, S. Li, K. M. Smedley, and S. Singer, "A family of two-switch boosting switched-capacitor converters," *IEEE Trans. Power Electron.*, vol. 30, no. 10, pp. 5413–5424, Oct. 2015.

[92] S. Li, B. Wu, K. Smedley, and S. Singer, "Analysis and design of a 1-kW 3X interleaved switched-capacitor DC-DC converter," in *Proc. IEEE Energy Convers. Congr. Expo.*, 2014, pp. 1692–1698.

[93] A. Sarafianos and M. Steyaert, "Fully integrated wide input voltage range capacitive DC-DC converters: The folding Dickson converter," *IEEE J. Solid-State Circuits*, vol. 50, no. 7, pp. 1560–1570, Jul. 2015.

[94] M. Amara and G. Chowdary, "A multi-ratio helical ladder switched-capacitor DC-DC converter for low power sensor nodes," *IEEE Trans. Circuits Syst. II, Exp. Briefs*, vol. 70, no. 10, pp. 3912–3916, Oct. 2023, doi: 10.1109/TCSII.2023.3290120.

[95] M. M. Henriksen, D. Ø. Larsen, and P. L. Muntal, "A design methodology for high-voltage, highly-integrated switched-capacitor power converters, and implementation at 48 V-12 V, 23 W/cm^3 and 93.5% peak efficiency," *IEEE Trans. Power Electron.*, vol. 38, no. 10, pp. 12254–12264, Oct. 2023, doi: 10.1109/TPEL.2023.3288592.

[96] D. Gunasekaran, L. Qin, U. Karki, Y. Li, and F. Z. Peng, "A variable (n/m) X switched capacitor DC–DC converter," *IEEE Trans. Power Electron.*, vol. 32, no. 8, pp. 6219–6235, Aug. 2017.

[97] R. L. da Silva, T. B. Lazzarin, and I. Barbi, "Reduced switch count step-up/step-down switched-capacitor three-phase AC–AC converter," *IEEE Trans. Ind. Electron.*, vol. 65, no. 11, pp. 8422–8432, Nov. 2018.

[98] T. B. Lazzarin, R. L. Andersen, and I. Barbi, "A switched-capacitor three-phase AC–AC converter," *IEEE Trans. Ind. Electron.*, vol. 62, no. 2, pp. 735–745, Feb. 2015.

[99] Y. Zhai, Y. Wang, Y. Guan, D. Xu, and H. Ma, "Design of a high step-down hybrid switched-capacitor converter," in *Proc. IEEE Int. Power Electron. Appl. Conf. Expo.*, 2022, pp. 795–800.

[100] M. V. Soares, G. Lambert, and Y. Rômulo de Novaes, "Hybrid switched capacitor DC-DC converter based on MMC," in *Proc. IEEE 15th Braz. Power Electron. Conf. 5th IEEE Southern Power Electron. Conf.*, 2019, pp. 1–6.

[101] J. Chen, K. Ding, Y. Zhong, F. Deng, and S. Abulanwar, "A double input-parallel-output-series hybrid switched-capacitor boost converter," *Chin. J. Elect. Eng.*, vol. 6, no. 4, pp. 15–27, Dec. 2020.

[102] A. Dago, M. Leoncini, S. Saggini, S. Levantino, and M. Ghioni, "Hybrid resonant switched-capacitor converter for 48–3.4 V direct conversion," *IEEE Trans. Power Electron.*, vol. 37, no. 11, pp. 12998–13002, Nov. 2022.

[103] M. S. Dall'Asta, I. Barbi, and T. B. Lazzarin, "AC–AC hybrid boost switched-capacitor converter," *IEEE Trans. Power Electron.*, vol. 35, no. 12, pp. 13115–13125, Dec. 2020.

[104] Z. Ye, Y. Lei, and R. C. N. Pilawa-Podgurski, "The cascaded resonant converter: A hybrid switched-capacitor topology with high power density and efficiency," *IEEE Trans. Power Electron.*, vol. 35, no. 5, pp. 4946–4958, May 2020.

[105] S. Li, N. Zhang, S. Zheng, W. Xie, and K. Smedley, "A Dickson resonant switched-capacitor converter with 'indirect' resonant core and continuous conversion ratio," in *Proc. IEEE Appl. Power Electron. Conf. Expo.*, 2019, pp. 2218–2222.

[106] N. B. Sagpazar, W. Cho, K. Kim, and S. Choi, "Three-level resonant switched capacitor boost converter," in *Proc. 10th Int. Conf. Power Electron. Energy Convers. Conf. Expo Asia*, 2019, pp. 2868–2873.

[107] Y. Dong-Ying, K. Shih-Hao, S. Yong-Long, C. Huang-Jen, L. Kuo-Chi, and Y. Ta-Yung, "An improved 48-to-12V series-parallel resonant switched-capacitor converter for data center applications," in *Proc. IEEE Int. Future Energy Electron. Conf.*, 2021, pp. 1–6.

[108] H. Setiadi and H. Fujita, "Control and performance of new asymmetrical operation for switched-capacitor-based resonant converters," in *Proc. Int. Power Electron. Conf. Energy Convers. Conf. Expo Asia*, 2018, pp. 626–631.

[109] S. Li, Y. Zheng, B. Wu, and K. M. Smedley, "A family of resonant two-switch boosting switched-capacitor converter with ZVS operation and a wide line regulation range," *IEEE Trans. Power Electron.*, vol. 33, no. 1, pp. 448–459, Jan. 2018.

[110] S. Li, S. Liang, Z. Li, W. Xie, P. Jia, and J. Yao, "A bidirectional resonant two-switch boosting switched-capacitor converter with phase-shift modulation," in *Proc. IEEE Appl. Power Electron. Conf. Expo.*, 2020, pp. 56–60.

[111] S. Li, C. Hao, W. Ding, S. Zheng, S. Zou, and G. Zhang, "Series-parallel multiresonant switched-capacitor converters and the optimal operation region," *IEEE Trans. Ind. Appl.*, vol. 59, no. 5, pp. 5971–5988, Sep./Oct. 2023.

[112] Z. Shan, X. Ding, J. Jatskevich, and C. K. Tse, "Synthesis of multi-input multi-output DC/DC converters without energy buffer stages," *IEEE Trans. Circuits Syst. II, Exp. Briefs*, vol. 68, no. 2, pp. 712–716, Feb. 2021.

[113] J. He, Y. Ye, and X. Wang, "ZVS and inrush charging current suppression design for switched-capacitor multilevel inverters," *IEEE Trans. Power Electron.*, vol. 38, no. 9, pp. 10611–10616, Sep. 2023, doi: 10.1109/TPEL.2023.3290570.

[114] P. H. A. Miranda, E. M. Sá, F. W. G. Rodrigues, and F. L. M. Antunes, "Single-stage three-phase AC-DC resonant switched capacitor LED driver without electrolytic capacitor and reduced number of controlled switches," *IEEE Trans. Circuits Syst. I, Regular Papers*, vol. 67, no. 12, pp. 5675–5686, Dec. 2020.

[115] H. Chung, "Design and analysis of quasi-switched-capacitor step-up DC/DC converters," in *Proc. IEEE Int. Symp. Circuits Syst.*, 1998, pp. 438–441.

[116] H. Chung and Y. K. Mok, "Development of a switched-capacitor DC/DC boost converter with continuous input current waveform," *IEEE Trans. Circuits Syst. I, Fundam. Theory Appl.*, vol. 46, no. 6, pp. 756–759, Jun. 1999.

[117] X. Zhang, C. Yao, F. Guo, L. Fu, and J. Wang, "A family of quasi-switched-capacitor converters," in *Proc. IEEE Conf. Expo Transp. Electrific. Asia-Pac.*, 2014, pp. 1–6.

[118] H. Chung, O. B., and A. Ioinovici, "Switched-capacitor-based DC-to-DC converter with improved input current waveform," in *Proc. IEEE Int. Symp. Circuits Syst.*, 1996, pp. 541–544.

[119] Y. Li, X. Lyu, D. Cao, S. Jiang, and C. Nan, "A high efficiency resonant switched-capacitor converter for data center," in *Proc. IEEE Energy Convers. Congr. Expo.*, 2017, pp. 4460–4466.

[120] S. Webb and Y.-F. Liu, "A novel intermediate bus converter topology for cutting edge data center applications," *Chin. J. Elect. Eng.*, vol. 6, no. 4, pp. 3–14, Dec. 2020.

[121] M. Ursino, R. Rizzolatti, G. Deboy, S. Saggini, and K. Zufferli, "High density hybrid switched capacitor sigma converter for data center applications," in *Proc. IEEE Appl. Power Electron. Conf. Expo.*, 2022, pp. 35–39.

[122] Z. Ye, Y. Lei, and R. C. N. Pilawa-Podgurski, "A 48-to-12 V cascaded resonant switched-capacitor converter for data centers with 99% peak efficiency and 2500 W/in^3 power density," in *Proc. IEEE Appl. Power Electron. Conf. Expo.*, 2019, pp. 13–18.

[123] W. Qian, H. Cha, F. Z. Peng, and L. M. Tolbert, "55-kW variable 3X DC-DC converter for plug-in hybrid electric vehicles," *IEEE Trans. Power Electron.*, vol. 27, no. 4, pp. 1668–1678, Apr. 2012.

[124] A. Janabi and B. Wang, "Switched-capacitor voltage boost converter for electric and hybrid electric vehicle drives," *IEEE Trans. Power Electron.*, vol. 35, no. 6, pp. 5615–5624, Jun. 2020.

[125] J. Elmes, R. Kersten, I. Batarseh, M. Pepper, and K. Mansfield, "Modular bidirectional DC-DC converter for hybrid/electric vehicles with variable-frequency interleaved soft-switching," in *Proc. IEEE Veh. Power Propulsion Conf.*, 2009, pp. 448–454.

[126] Y. Zhang, S. Gao, S. Jing, and X. Huang, "Soft-switching operation with a variable switching frequency control for switched-quasi-Z-source bidirectional DC–DC converter in EVs," *IEEE Trans. Ind. Electron.*, vol. 70, no. 1, pp. 384–395, Jan. 2023.

[127] J. Han, A. von Jouanne, and G. C. Temes, "A new approach to reducing output ripple in switched-capacitor-based step-down DC–DC converters," *IEEE Trans. Power Electron.*, vol. 21, no. 6, pp. 1548–1555, Nov. 2006.

[128] E. Abramov, A. Cervera, and M. M. Peretz, "Optimal design of a voltage regulator based on gyrator switched-resonator converter IC," *IEEE J. Emerg. Sel. Topics Power Electron.*, vol. 6, no. 2, pp. 549–562, Jun. 2018.

[129] C. Schaef, K. Kesarwani, and J. T. Stauth, "20.2 A variable-conversion-ratio 3-phase resonant switched capacitor converter with 85% efficiency at 0.91W/mm2 using 1.1nH PCB-trace inductors," in *Proc. IEEE Int. Solid-State Circuits Conf. Dig. Tech. Papers*, 2015, pp. 1–3.

[130] C. Schaef and J. T. Stauth, "A highly integrated series–parallel switched-capacitor converter with 12 V input and quasi-resonant voltage-mode regulation," *IEEE J. Emerg. Sel. Topics Power Electron.*, vol. 6, no. 2, pp. 456–464, Jun. 2018.

[131] H.-K. Kwan, D. C. W. Ng, and V. W. K. So, "Design and analysis of dual-mode digital-control step-up switched-capacitor power converter with pulse-skipping and numerically controlled oscillator-based frequency modulation," *IEEE Trans. Very Large Scale Integr. Syst.*, vol. 21, no. 11, pp. 2132–2140, Nov. 2013.

[132] V. E. Shunkov, O. N. Kus, V. Y. Prokopyev, V. A. Butuzov, and Y. I. Bocharov, "Fully integrated switched-capacitor voltage converter with regulated output," in *Proc. Moscow Workshop Electron. Netw. Technol.*, 2018, pp. 1–4.

[133] M. Uno, H. Sato, and S. Oyama, "Switched capacitor-based modular differential power processing architecture for large-scale photovoltaic systems under partial shading," *IEEE Trans. Energy Convers.*, vol. 37, no. 3, pp. 1545–1556, Sep. 2022.

[134] S. R. Kukunuru, Y. Naeimi, and L. G. Salem, "A series-parallel switched-photovoltaic DC–DC converter," *IEEE J. Solid-State Circuits*, vol. 58, no. 3, pp. 742–756, Mar. 2023.

[135] M. Uno and M. Yamamoto, "Switched capacitor-based PWM converter integrating string converter and voltage equalizer for photovoltaic strings under partial shading," in *Proc. TENCON IEEE Region 10 Conf.*, 2017, pp. 1058–1063.

[136] K. O. Htet, H. Fan, and H. Heidari, "Switched capacitor DC-DC converter for miniaturised wearable systems," in *Proc. IEEE Int. Symp. Circuits Syst.*, 2018, pp. 1–5.

[137] D. Kilani, B. Mohammad, M. Alhawari, H. Saleh, and M. Ismail, "A dual-output switched capacitor DC–DC buck converter using adaptive time multiplexing technique in 65-nm CMOS," *IEEE Trans. Circuits Syst. I, Regular Papers*, vol. 65, no. 11, pp. 4007–4016, Nov. 2018.

[138] C. K. Teh and A. Suzuki, "12.3 A 2-output step-up/step-down switched-capacitor DC-DC converter with 95.8% peak efficiency and 0.85-to-3.6V input voltage range," in *Proc. IEEE Int. Solid-State Circuits Conf.*, 2016, pp. 222–223.

[139] D. Kilani, M. Alhawari, B. Mohammad, H. Saleh, and M. Ismail, "An efficient switched-capacitor DC-DC buck converter for self-powered wearable electronics," *IEEE Trans. Circuits Syst. I, Regular Papers*, vol. 63, no. 10, pp. 1557–1566, Oct. 2016.

[140] O. Al-Terkawi Hasib, M. Sawan, and Y. Savaria, "A low-power asynchronous step-down DC–DC converter for implantable devices," *IEEE Trans. Biomed. Circuits Syst.*, vol. 5, no. 3, pp. 292–301, Jun. 2011.

[141] J. W. Kimball and P. T. Krein, "Analysis and design of switched capacitor converters," in *Proc. 20th Annu. IEEE Appl. Power Electron. Conf. Expo.*, 2005, pp. 1473–1477.

[142] J. W. Kimball, P. T. Krein, and K. R. Cahill, "Modeling of capacitor impedance in switching converters," *IEEE Power Electron. Lett.*, vol. 3, no. 4, pp. 136–140, Dec. 2005.

[143] M. Evzelman and S. Ben-Yaakov, "Average-current-based conduction losses model of switched capacitor converters," *IEEE Trans. Power Electron.*, vol. 28, no. 7, pp. 3341–3352, Jul. 2013.

[144] R. J. Dirkman, "Generalized state space averaging," in *Proc. IEEE Power Electron. Spec. Conf.*, 1983, pp. 283–294.

[145] M. D. Seeman and S. R. Sanders, "Analysis and optimization of switched capacitor DC-DC converters," *IEEE Trans. Power Electron.*, vol. 23, no. 2, pp. 841–851, Mar. 2008.

[146] M. Krstic, S. Eren, and P. Jain, "Curvature-based average modeling of switched-capacitor converters," *IEEE J. Emerg. Sel. Topics Power Electron.*, vol. 9, no. 5, pp. 5929–5940, Oct. 2021.

[147] H. Xie and R. Li, "Simplified modeling and control of a GaN switched-capacitor converters with phase shift modulation," *IEEE Trans. Power Electron.*, vol. 36, no. 12, pp. 14550–14566, Dec. 2021.

[148] Y. Ye and K. W. E. Cheng, "Voltage-gap modeling method for single stage switched-capacitor converters," *IEEE J. Emerg. Sel. Topics Power Electron.*, vol. 2, no. 4, pp. 808–813, Dec. 2014.

[149] J. M. Henry and J. W. Kimball, "Practical performance analysis of complex switched-capacitor converters," *IEEE Trans. Power Electron.*, vol. 26, no. 1, pp. 127–136, Jan. 2011.

[150] J. M. Henry and J. W. Kimball, "Switched-capacitor converter state model generator," *IEEE Trans. Power Electron.*, vol. 26, no. 1, pp. 127–136, Jan. 2011.

[151] B. Wu, S. Li, K. M. Smedley, and S. Singer, "Analysis of high power switched capacitor converter regulation based on charge-balance transient-calculation method," *IEEE Trans. Power Electron.*, vol. 31, no. 5, pp. 3482–3494, May 2016.

[152] B. Wu, S. Li, K. Smedley, and S. Singer, "A family of two-switch boosting switched-capacitor converters," *IEEE Trans. Power Electron.*, vol. 30, no. 10, pp. 5413–5424, Oct. 2015.

[153] S. V. Cheong, S. H.Chung, and A. Ioinovici, "Development of power electronics converters based on switched-capacitor circuits," in *Proc. IEEE Int. Symp. Circuits Syst.*, 1992, pp. 1907–1910.

[154] T. Suetsugu, "Novel PWM control method of switched capacitor DC-DC converter," in *Proc. IEEE Int. Symp. Circuits Syst.*, 1998, pp. 454–457.

[155] M. Veerachary, "Control of switched capacitor step-down buck converter," in *Proc. IECON 32nd Annu. Conf. IEEE Ind. Electron.*, 2006, pp. 2073–2076.

[156] H. Chung and Y. K. Mok, "Development of a switched-capacitor DC/DC boost converter with continuous input current waveform," *IEEE Trans. Circuits Syst. I, Fundam. Theory Appl.*, vol. 46, no. 6, pp. 756–759, Jun. 1999.

[157] H. S. H. Chung, S. Y. R. Hui, S. C. Tang, and A. Wu, "On the use of current control scheme for switched-capacitor DC/DC converters," *IEEE Trans. Ind. Electron.*, vol. 47, no. 2, pp. 238–244, Apr. 2000.

[158] H. Chung, "Design and analysis of quasi switched-capacitor step-up DC/DC converters," in *Proc. IEEE Int. Symp. Circuits Syst.*, 1998, pp. 438–441.

[159] Z. Xiao, A. K. Bui, and L. Siek, "A hysteretic switched-capacitor DC–DC converter with optimal output ripple and fast transient response," *IEEE Trans. Very Large Scale Integr. Syst.*, vol. 25, no. 11, pp. 2995–3005, Nov. 2017.

[160] T. McRae, T. Souvignet, B. Eleftheriades, A. Prodić, and B. Allard, "Flying capacitor voltage programed mode control for switched-capacitor converters," *IEEE J. Emerg. Sel. Topics Power Electron.*, vol. 8, no. 3, pp. 2082–2094, Sep. 2020.

[161] X. Yang et al., "Improved phase shift control for SiC-MOSFET based resonant switched-capacitor converter with parasitics consideration," *IEEE Trans. Ind. Appl.*, vol. 56, no. 4, pp. 3995–4006, Jul./Aug. 2020.

[162] K. Sano and H. Fujita, "Performance of a high-efficiency switched-capacitor-based resonant converter with phase-shift control," *IEEE Trans. Power Electron.*, vol. 26, no. 2, pp. 344–354, Feb. 2011.

[163] S.-C. Tan et al., "Nonlinear control of switched-capacitor converter using sliding mode control approach," in *Proc. IEEE Power Electron. Spec. Conf.*, 2008, pp. 372–377.

[164] S.-C. Tan, S. Bronstein, M. Nur, Y. M. Lai, A. Ioinovici, and C. K. Tse, "Variable structure modeling and design of switched-capacitor converters," *IEEE Trans. Circuits Syst. I, Regular Papers*, vol. 56, no. 9, pp. 2132–2142, Sep. 2009.

[165] L. Yang, W. Zhang, X. Zhang, and G. P. Li, "Nonlinear variable frequency control of high power switched-capacitor converter," in *Proc. IEEE 8th Int. Power Electron. Motion Control Conf. Energy Convers. Conf. Expo Asia*, 2016, pp. 3472–3476.

[166] L. Yang, X. Zhang, B. Wu, K. M. Smedley, and G. P. Li, "Constant on-time variable frequency one-cycle control for switched-capacitor converter," in *Proc. IEEE Transp. Electrific. Conf. Expo*, 2016, pp. 1–6.

[167] L. Yang, B. Wu, X. Zhang, K. Smedley, and G.-P. Li, "Dynamic modeling and analysis of constant on time variable frequency one-cycle control for switched-capacitor converters," *IEEE Trans. Circuits Syst. I, Regular Papers*, vol. 64, no. 3, pp. 630–641, Mar. 2017.

[168] X. Li, X. Wu, F. Deng, W. Li, and L. Yang, "Constant on-time variable frequency control for a novel switched-capacitor converter," in *Proc. 9th IEEE Int. Symp. Power Electron. Distrib. Gener. Syst.*, 2018, pp. 1–8.

[169] S. R. Sanders, E. Alon, H.-P. Le, M. D. Seeman, M. John, and V. W. Ng, "The road to fully integrated DC–DC conversion via the switched-capacitor approach," *IEEE Trans. Power Electron.*, vol. 28, no. 9, pp. 4146–4155, Sep. 2013.

[170] J. Jiang, X. Liu, W.-H. Ki, P. K. T. Mok, and Y. Lu, "Circuit techniques for high efficiency fully-integrated switched-capacitor converters," *IEEE Trans. Circuits Syst. II, Exp. Briefs*, vol. 68, no. 2, pp. 556–561, Feb. 2021.

[171] L. Geng, Z. Chen, and J. Liu, "Design of a hybrid monolithic integrated switched capacitor DC-DC step-up converter," in *Proc. 3rd Int. Power Electron. Motion Control Conf.*, 2000, pp. 263–266.

[172] K. Datta, P. H. McLaughlin, and J. T. Stauth, "A fully-integrated direct-conversion resonant switched capacitor converter with modular multi-winding current ballasting," in *Proc. IEEE Custom Integr. Circuits Conf.*, 2023, pp. 1–2.

[173] T. Van Daele and F. Tavernier, "Fully integrating a 400 V-to-12 V DC–DC converter in high-voltage CMOS," *IEEE J. Solid-State Circuits*, vol. 58, no. 3, pp. 732–741, Mar. 2023.

[174] L. Ziwei, W. Xuezhi, W. Jing, Q. Jingjing, J. Long, and X. Wenzheng, "Design of magnetic integrated inductor for resonant switched capacitor converter," *Trans. China Electrotech. Soc.*, vol. 37, no. 24, pp. 6230–6238, 2022.

[175] A. Gehl et al., "A 2-8V Vin 670mA scalable multi-ratio SC DCDC converter for MCU integration in 28nm CMOS achieving 91% peak efficiency," in *Proc. IEEE 49th Eur. Solid State Circuits Conf.*, 2023, pp. 425–428.

[176] M. Qiu, M. Wei, X. Liu, H. Meng, and D. Cao, "A family of novel switch capacitor based integrated matrix autotransformer LLC converter for data center application," in *Proc. IEEE Green Technol. Conf.*, 2023, pp. 118–122.

[177] Y. Zhu, T. Ge, Z. Ye, and R. C. N. Pilawa-Podgurski, "A Dickson-squared hybrid switched-capacitor converter for direct 48 V to point-of-load conversion," in *Proc. IEEE Appl. Power Electron. Conf. Expo.*, 2022, pp. 1272–1278.

[178] M. Kumar, V. K. Yadav, and A. K. Verma, "Switched capacitor based high gain boost converter for renewable energy application," *IEEE J. Emerg. Sel. Topics Ind. Electron.*, vol. 4, no. 3, pp. 818–826, Jul. 2023.

[179] Y. Mahnashi, "A new approach to improve the voltage conversion ratio in topological switched-capacitor DC–DC converters using negator stage," *IEEE Trans. Circuits Syst. II, Exp. Briefs*, vol. 70, no. 4, pp. 1465–1469, Apr. 2023.

[180] I.-B. Kong, W.-S. Kim, and S.-W. Lee, "A novel high-voltage-gain quasi-resonant DC–DC converter with active-clamp and switched-capacitor techniques," *IEEE Trans. Power Electron.*, vol. 38, no. 6, pp. 7810–7820, Jun. 2023.

[181] S. Ra and Asharani, "Improved hybrid switched capacitor/inductor converters for high step-up conversion," in *Proc. IEEE North Karnataka Subsection Flagship Int. Conf.*, 2022, pp. 1–6.

[182] T. Nouri, M. Shaneh, M. Benbouzid, and N. V. Kurdkandi, "An interleaved ZVS high step-up converter for renewable energy systems applications," *IEEE Trans. Ind. Electron.*, vol. 69, no. 5, pp. 4786–4800, May 2022.

[183] R. Rizzolatti, C. Rainer, S. Saggini, and M. Ursino, "High density hybrid switched capacitor converter for data-center application," in *Proc. IEEE Appl. Power Electron. Conf. Expo.*, 2021, pp. 1288–1293.

[184] R. A. Abramson, Z. Ye, T. Ge, and R. C. N. Pilawa-Podgurski, "A high performance 48-to-6 V multi-resonant cascaded series-parallel (CaSP) switched-capacitor converter," in *Proc. IEEE Appl. Power Electron. Conf. Expo.*, 2021, pp. 1328–1334.

[185] M. R. Khan, K. Wei, X. Zhang, and C. Huang, "A single-inductor 4-phase hybrid switched-capacitor topology for integrated 48V-to-1V DC-DC converters," in *Proc. IEEE Int. Symp. Circuits Syst.*, 2023, pp. 1–5.

[186] Y. Zhu, T. Ge, N. M. Ellis, L. Horowitz, and R. C. N. Pilawa-Podgurski, "A 500-A/48-to-1-V switching bus converter: A hybrid switched-capacitor voltage regulator with 94.7% peak efficiency and 464-W/in3 power density," in *Proc. IEEE Appl. Power Electron. Conf. Expo.*, 2023, pp. 1989–1996.

[187] M. Sharifzadeh, M. Ahmadijokani, M. Mehrasa, M. Sadabadi, and K. Al-Haddad, "Novel switched-capacitor compact multilevel converter based on packed E-cell design with fault tolerant operation," in *Proc. IECON 47th Annu. Conf. IEEE Ind. Electron. Soc.*, 2021, pp. 1–6.

[188] J. Ebrahimi, S. Shahnooshi, S. Eren, H. Karshenas, and A. Bakhshai, "Optimized switching frequency voltage balancing schemes for flying capacitor based multilevel converters," *IEEE Trans. Ind. Electron.*, vol. 70, no. 11, pp. 10775–10788, Nov. 2023.

[189] X. Zhang et al., "A 12/24 V-input HV-LV-separated hybrid SC PoL converter with 355 mW/mm^3 power density at 3 a load current and 15.2 mm^3 power passives," *IEEE Trans. Power Electron.*, vol. 38, no. 12, pp. 15109–15114, Dec. 2023.

[190] L. Yang et al., "Single wire capacitive wireless power transfer system for wearable biomedical sensors based on flexible graphene film material," *IEEE Trans. Biomed. Circuits Syst.*, vol. 16, no. 6, pp. 1337–1347, Dec. 2022.

[191] Y. Wu and X. Du, "A VEN condition monitoring method of DC-link capacitors for power converters," *IEEE Trans. Ind. Electron.*, vol. 66, no. 2, pp. 1296–1306, Feb. 2019.

[192] Y. Ran, Z. Meimei, L. Hui, L. Wei, W. Xiao, and L. Haiyang, "Reliability modeling and analysis on metallized film capacitors for MMC," in *Proc. 10th Int. Conf. Power Electron. Energy Convers. Conf. Expo Asia*, 2019, pp. 1854–1860.

[193] T. Ge, Z. Ye, and R. C. N. Pilawa-Podgurski, "Geometrical state-plane analysis of resonant switched-capacitor converters: Demonstration on the cascaded multiresonant converter," *IEEE Trans. Power Electron.*, vol. 38, no. 9, pp. 11125–11140, Sep. 2023.

[194] S. Coday, E. Krause, M. E. Blackwell, N. M. Ellis, A. Barchowsky, and R. C. N. Pilawa-Podgurski, "Design and implementation of a GaN-based capacitively-isolated hybrid Dickson switched-capacitor DC-DC converter for space applications," in *Proc. IEEE Appl. Power Electron. Conf. Expo.*, 2023, pp. 3154–3159.

Ting Yang was born in Shaanxi province China, in 1987. He received the B.S. degree from Dalian University, Dalian, China, in 2010, the M.S. degree from Yangzhou University, Yangzhou, China, in 2012, and the Ph.D. degree from Gunma University, Maebashi, Japan, in 2021.

He is currently working with Yulin University, Yulin, China. His research interests include power electronics and motor drives.

Lei Yang (Senior Member, IEEE) was born in Henan, China, in 1986. He received the B.S. degree in electric and information engineering from Information Engineering University, Zhengzhou, China, in 2011, and the M.S. degree in signal and information processing and the Ph.D. degree in electrical engineering from Northwestern Polytechnical University, Xi'an, China, in 2014 and in 2017, respectively.

He is currently an Assistant Professor with the Xi'an University of Technology, Xi'an, China. From 2014 to 2016, he was a visiting student with the University of California, Irvine, CA, USA. His research interests include nonlinear control methods, wireless power transfer systems, underwater communication and power deliver systems, switched capacitor converters, dc–dc converter, power source of electrical vehicles, and renewable energy integration.

Bin Wu (Student Member, IEEE) was born in Zhejiang, China. He received the Ph.D. degree in power electronics from the University of California at Irvine, Irvine, CA, USA, in 2016.

From 2016 to 2017, he was a Postdoctoral Research Associate with The University of Maryland, College Park, MD, USA. After that, he was a System Engineer with Maxim Integrated, San Jose, CA, USA, and a Staff Applications Engineer with Analog Devices, Inc., Norwood, MA, USA. He is currently a Hardware Engineer with Google, Inc., Mountain View, CA, USA. His research interests include switched capacitor converters, electrical vehicle chargers, power electronics modeling, high-gain dc–dc converter, renewable energy, and consumer battery systems.

Liangzong He (Member, IEEE) was born in Hunan, China, in 1984. He received the B.Sc. degree from Jilin University, Changchun, China, in 2006, and the Ph.D. degree from the Huazhong University of Science and Technology, Wuhan, China, in 2012, both in electrical engineering.

From 2009 to 2011, he was a joint Ph.D. education student with Michigan State University, East Lansing, MI, USA. In 2012, he was with Xiamen University, Xiamen, China, as an Assistant Professor, and has been a Professor there since 2019. His research interests include high-efficient power conversion, switched-capacitor converters, Z-source converters, wireless power transmission, and stability analysis and low-frequency ripple suppression.

Yuanqi Zhang was born in Shaanxi, China, in 1999. He is currently working toward the master's degree in electrical engineering and automation with the Xi'an University of Technology, Xi'an, China.

He is currently a member of the Research and Development Team of the underwater wireless power transfer system of the Xi'an University of Technology. His main research direction is the control strategy of wireless power transmission system and bidirectional dc–dc converter.

Xinze Chen was born in Shaanxi, China, in 2000. He received the B.S. degree in electrical engineering and automation in 2022 from the Xi'an University of Technology, Xi'an, China, where he is currently working toward the master's degree.

He is currently a member of wireless power transfer system of the Xi'an University of Technology. His research interests include dc–dc converter and wireless power transmission system.

Baoxiang Feng was born in Shaanxi, China. He received the M.S. degree in electrical engineering and automation from the Xi'an University of Technology, Xi'an, China, in 2021.

He is currently a member of the Research and Development Team of the underwater wireless power transfer system of the Xi'an University of Technology. His research interests include circuit design, wireless power transfer systems, switched-capacitor converters, and nonlinear control method.

Xiaojie Li was born in Shaanxi Province, China, in 1998. She received the B.S. degree in electrical engineering and automation in 2019 from the Xi'an University of Technology, Xi'an, China, where she is currently working toward the M.S. degree.

Her research interests include the control strategy of wireless power transmission systems and bidirectional dc–dc converters.

Haibing Wen (Member, IEEE) received the B.S., M.S., and Ph.D. degrees from Northwestern Polytechnical University, Xi'an, China, in 2010, 2013, and 2021, respectively.

Since 2021, he has been a full-time Postdoctoral Research Fellow with the School of Electrical Engineering, Xi'an University of Technology, Xi'an, China. His research interests include wireless power transfer, including electromagnetic shielding and system optimization.

Jiaqiang Tian (Member, IEEE) received the B.S. degree in automation from Xi'an Technological University, Xi'an, China, in 2016, and the Ph.D. degree in control science and engineering from the University of Science and Technology of China, Hefei, China, in 2021, respectively.

From 2021 to 2022, he was a full-time Lecturer with the Xi'an University of Technology, Xi'an, China. He has been a full-time Postdoctoral Research Fellow with Anhui University since October 2022. His research interests include energy storage modeling, battery fault diagnosis and energy management, and optimal scheduling of integrated energy systems.

Yaopeng Zhao (Member, IEEE) was born in Shaanxi, China, in 1989. He received the B.S. and M.S. degrees from the School of Power and Energy, Xi'an Jiao Tong University, Xi'an, China, in 2010 and 2013, respectively, and received the Ph.D. degree from the School of Microelectronics, Xidian University, Xi'an, China, in 2021.

He is currently working as an Assistant Professor with the Xi'an University of Technology. His research interests include the design, packaging, and reliability testing of GaN power devices, as well as research on the applications in switching power supplies, inverters, and so on.

Mengying Hu was born in Hebei, China, in 1989. She received the B.S. degree in electrical engineering and automation and the M.S. degree in electrical engineering from the Xi'an University of Technology, Xi'an, China, in 2012 and 2015, respectively.

She is currently working as an Engineer with the Xi'an University of Technology. Her research interests include virtual simulation experiment system, motor drive and control, wind power generation system, and wind power forecasting.

Jingjing Huang (Member, IEEE) received the B.S. degree from the Henan University of Science and Technology, Luoyang, China, in 2008, and the Ph.D. degree from Xi'an Jiaotong University, Xi'an, China, in 2014, both in electrical engineering.

From 2014 to 2016, she was a full-time Lecturer with the Xi'an University of Technology, Xi'an, China. From 2016 to 2019, she was a full-time Postdoctoral Research Fellow with Nanyang Technological University, Singapore. She is currently an Associate Professor with the School of Electronic and Information Engineering, Xi'an Jiaotong University. Her research interests include renewable energy systems, high-frequency transformers, hybrid ac/dc microgrids, and high-power converters.

Darui Zhu received the B.S. degree in automation and the M.S. degree in detection technology and automatic equipment, both from Xi'an Polytechnic University, Xi'an, China, in 2007 and 2010, respectively, and the Ph.D. degree in electrical engineering from Xi'an Jiaotong University, Xi'an, China, in 2014.

He is currently a Lecturer with the School of Electrical Engineering, Xi'an University of Technology. His research interests include the modeling of nonlinear systems, complex network theory, and power system security analysis.

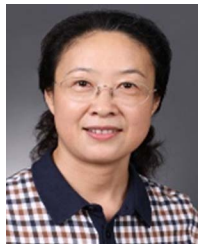

Aimin Zhang (Member, IEEE) received the B.S., M.S., and Ph.D. degrees in control science and engineering from Xi'an Jiaotong University, Xi'an, China, in 1983, 1989, and 2008, respectively.

Since 1983, she has been with the School of Electronic and Information Engineering, Xi'an Jiaotong University, where she is currently a Professor. Her current research interests include adaptive control, new energy control systems, and embedded intelligent measurement and control systems.

Xiangqian Tong (Member, IEEE) was born in Shaanxi Province, China, in 1961. He received the B.S. degree in electrical engineering from the Shaanxi Institute of Technology, Hanzhong, China, and the M.S. degree in electrical engineering from the Xi'an University of Technology, Xi'an, China, in 1983 and 1989, respectively, and the Ph.D. degree in electrical engineering from Xi'an Jiaotong University, Xi'an, China, in 2006.

He joined the Xi'an University of Technology in 1989. Since 2002, he has been a Professor and the Academic Leader of electrical engineering with the Xi'an University of Technology. His research interests include the application of power electronics in power systems and control of power quality, especially the power filter, static synchronous compensator, and high-voltage direct current.